Fungal Genetics and Biology 49 (2012) 589–601

Contents lists available at SciVerse ScienceDirect

Fungal Genetics and Biology

journal homepage: www.elsevier.com/locate/yfgbi

Technological Advancement

Expression of the Cameleon calcium biosensor in fungi reveals distinct Ca^{2+} signatures associated with polarized growth, development, and pathogenesis

Hye-Seon Kim [a,1], Kirk J. Czymmek [b,c,*,1], Agam Patel [c], Shannon Modla [c], Anja Nohe [b], Randall Duncan [b], Simon Gilroy [d], Seogchan Kang [a,*]

[a] Department of Plant Pathology, The Pennsylvania State University, University Park, PA 16802, United States
[b] Department of Biological Sciences, University of Delaware, Newark, DE 19716, United States
[c] Delaware Biotechnology Institute, Newark, DE 19711, United States
[d] Department of Botany, University of Wisconsin, Madison, WI 53706, United States

ARTICLE INFO

Article history:
Received 24 January 2012
Accepted 24 May 2012
Available online 7 June 2012

Keywords:
Calcium signaling
Cameleon
Fluorescent protein
Biosensor
Polarized tip growth
Pulsatile calcium signature

ABSTRACT

Calcium is a universal messenger that translates diverse environmental stimuli and developmental cues into specific cellular and developmental responses. While individual fungal species have evolved complex and often unique biochemical and structural mechanisms to exploit specific ecological niches and to adjust growth and development in response to external stimuli, one universal feature to all is that Ca^{2+}-mediated signaling is involved. The lack of a robust method for imaging spatial and temporal dynamics of subcellular Ca^{2+} (i.e., "Ca^{2+} signature"), readily available in the plant and animal systems, has severely limited studies on how this signaling pathway controls fungal growth, development, and pathogenesis. Here, we report the first successful expression of a FRET (Förster Resonance Energy Transfer)-based Ca^{2+} biosensor in fungi. Time-lapse imaging of *Magnaporthe oryzae*, *Fusarium oxysporum*, and *Fusarium graminearum* expressing this sensor showed that instead of a continuous gradient, the cytoplasmic Ca^{2+} ($[Ca^{2+}]_c$) change occurred in a pulsatile manner with no discernable gradient between pulses, and each species exhibited a distinct Ca^{2+} signature. Furthermore, occurrence of pulsatile Ca^{2+} signatures was age and development dependent, and major $[Ca^{2+}]_c$ transients were observed during hyphal branching, septum formation, differentiation into specialized plant infection structures, cell–cell contact and *in planta* growth. In combination with the sequenced genomes and ease of targeted gene manipulation of these and many other fungal species, the data, materials and methods developed here will help understand the mechanism underpinning Ca^{2+}-mediated control of cellular and developmental changes, its role in polarized growth forms and the evolution of Ca^{2+} signaling across eukaryotic kingdoms.

1. Introduction

Ca^{2+} translates external stimuli into specific cellular or developmental responses in organisms ranging from unicellular microbes to animals and plants (Clapham, 2007; Dodd et al., 2010; Nguyen et al., 2008). How this simple and ubiquitous ion manages to perform evolutionary conserved signal processing, yet exquisitely fine-tuned for individual cell types and organisms, is one of the most extensively studied questions in cell biology. A prevailing model is that the influx and efflux of Ca^{2+} through several types of channels and transporters on organellar and plasma membranes in response to external stimuli define the spatial and temporal patterns of cytoplasmic Ca^{2+} ($[Ca^{2+}]_c$). Resulting "Ca^{2+} signatures" are decoded by coordinated actions of Ca^{2+}-binding proteins (CBPs), such as calmodulin (CaM), CaM-like proteins, calcineurin (a Ca^{2+} and CaM dependent phosphatase), Ca^{2+}-dependent protein kinases, certain cytoskeletal proteins and proteins that directly or indirectly interact with CBPs (e.g., kinases, transcription factors, and ion transporters), ultimately leading to specific cellular responses (Clapham, 2007; Dodd et al., 2010).

Relative to plants and animals, very little is known about the nature of Ca^{2+} signatures in fungi and how they are generated and change during growth and development. This disparity is in large part due to the lack of robust tools for imaging subcellular Ca^{2+} changes over time at the single cell level, which is required to correlate the function and activity of various Ca^{2+} signaling proteins with Ca^{2+} signatures. Although fluorescent dyes as Ca^{2+} indicators have been used in a few fungi (Nair et al., 2011; Read et al., 1992; Silverman-Gavrila and Lew, 2003), their utility is limited due to several technical difficulties and low resolution. The advent of

* Corresponding authors. Address: 304 Wolf Hall, Department of Biological Sciences, University of Delaware, Newark, DE 19716, United States. Fax: +1 302 831 2281 (K.J. Czymmek), fax: +1 814 863 7217 (S. Kang).
E-mail addresses: kirk@udel.edu (K.J. Czymmek), sxk55@psu.edu (S. Kang).
[1] These authors contributed equally to the work.

1087-1845/$ - see front matter © 2012 Elsevier Inc. All rights reserved.
http://dx.doi.org/10.1016/j.fgb.2012.05.011

gene cloning has resulted in several types of protein-based Ca^{2+} sensors as alternatives to fluorescent dyes (Demaurex, 2005; Knight et al., 1991b; Zhao et al., 2011). The aequorin gene from the jellyfish *Aequoria victoria* and its derivatives have been expressed successfully in bacteria and diverse eukaryotes including fungi for monitoring $[Ca^{2+}]_c$ (Knight et al., 1991a, 1991b; Nelson et al., 2004; Rogers et al., 2007). However, due to its weak signal, it is limited to observing $[Ca^{2+}]_c$ dynamics in populations of cells and subcellular imaging of Ca^{2+} is generally not practical.

The FRET (Förster Resonance Energy Transfer)-based Ca^{2+} sensors of the Cameleon family offer several advantages over aequorin and chemical dyes, such as higher resistance to bleaching, less auto-fluorescence and enhanced brightness (Borst et al., 2008; Horikawa et al., 2010; Nagai et al., 2004; Truong et al., 2001). Several versions of Cameleon have been produced (Demaurex, 2005), but they all consist of calmodulin (CaM) and the CaM-binding module M13 sandwiched between cyan (FRET donor) and yellow (acceptor) fluorescent proteins. In the absence of Ca^{2+}, the excitation of CFP results in the emission of cyan fluorescence. However, when the CaM module takes up four molecules of Ca^{2+} and interacts with M13, the resulting protein conformational change brings CFP into a more optimal position for FRET to occur to YFP. When this occurs, the excitation of CFP leads to an energy transfer to YFP, resulting in yellow fluorescence. This reversible interaction is detected by increased emission from YFP and a simultaneously decreased CFP emission, which can be used to monitor Ca^{2+} concentration changes in living cells via ratiometric imaging over time. Cameleon sensors have been successfully expressed in whole animals (Diegelmann et al., 2002; Hasan et al., 2004; Higashijima et al., 2003) and plants (Allen et al., 1999; Iwano et al., 2004; Kosuta et al., 2008; Monshausen et al., 2008). FRET-based Ca^{2+} sensors with a Ca^{2+} binding module different from that in Cameleons (Heim and Griesbeck, 2004; Palmer et al., 2004) as well as single fluorescent protein (FP)-based Ca^{2+} sensors (Nagai et al., 2001; Nakai et al., 2001; Souslova et al., 2007; Tallini et al., 2006; Tian et al., 2009) have also been developed as alternatives to Cameleons. However, the use of Cameleons or other types of FP-based sensors in any fungus has never been reported.

In this study, we imaged and compared the spatial and temporal $[Ca^{2+}]_c$ dynamics by expressing the Cameleon YC3.60 (Nagai et al., 2004) in three important plant pathogenic, filamentous fungi. *Magnaporthe oryzae* is a major foliar pathogen of rice and other monocot species (Talbot and Foster, 2001). *Fusarium oxysporum* causes wilts in many important crop plants, while *Fusarium graminearum* infects wheat and barley and produces toxic metabolites in infected grains (Desjardins, 2006; Ma et al., 2010). Their nature of Ca^{2+} dynamics during growth, differentiation or pathogenesis was compared. This major technical breakthrough provides a key missing tool for exploring the underpinning of fungal Ca^{2+} signaling and its evolution. All three species are amenable to targeted gene manipulations and have been sequenced (Coleman et al., 2009; Cuomo et al., 2007; Dean et al., 2005; Ma et al., 2010). Success in expressing YC3.60 will help us study how the Ca^{2+} signaling mechanism controls hyphal growth, development, pathogenesis, and responses to environmental stimuli.

2. Materials and methods

2.1. Fungal strains and growth conditions

F. oxysporum isolate O-685 (Kim et al., 2011) and *F. graminearum* PH-1 (Ma et al., 2010) were obtained from *Fusarium* Research Center at Penn State. *F. graminearum* strain GZ3639 (Bowden and Leslie, 1999) was obtained from Dr. Yin-Won Lee at Seoul National University. Cultures of *F. oxysporum* and *F. graminearum* stored at −80 °C in 20% glycerol were revitalized by inoculating them on solid minimal medium (Puhalla, 1985) and complete medium (Correll et al., 1987), respectively. Microconidia of *F. oxysporum* and macroconidia of *F. gramineraum* were produced by culturing in carboxymethyl cellulose broth (15 g CMC, 1 g yeast extract, 0.5 g $MgSO_4$, 1 g NH_4NO_3 and 1 g KH_2PO_4 per liter). *M. oryzae* isolate 4360–17-1 (Sweigard et al., 1995), which was stored in the form of dried culture on filter paper at −20 °C, was grown at 25 °C on oatmeal agar plate for 14 days to produce conidia. For genomic DNA extraction, fungal cultures were grown in potato dextrose broth. After filtering conidia through Miracloth (Calbiochem, La Jolla, CA), spores were harvested by centrifugation and washed twice with sterile water.

2.2. Construction of vectors

Escherichia coli strain DH5α was used for building and maintenance of the vector constructs used here. The sequences of all oligos used here are shown in Supplementary Table 1. The YC3.60 construct under the control of the 35S promoter in pGreenII (Monshausen et al., 2008) was digested with *Nco*I and *Xba*I to release the coding region of YC3.60. The *Fusarium verticillioides* elongation factor-1 alpha (*EF-1α*) gene promoter was amplified by PCR using the primers EF-*Eco*RI and EF-*Nco*I from pSK2325, a clone that carries a 670 bp *Eco*RI–*Nco*I fragment corresponding to this promoter. The amplified promoter was cloned into pGEM-TEasy (Promega, Madison, WI) and sequenced to verify the absence of mutations during PCR. The promoter ($\mathbf{P}_{EF\text{-}1\alpha}$) fragment (*Eco*RI–*Nco*I) and the coding region of YC3.60 ($\mathbf{C}_{YC3.60}$; *Nco*I–*Xba*I) were ligated between the *Eco*RI and *Xba*I sites of pSK1213, which carries the *Neurospora crassa* β-tubulin gene terminator ($\mathbf{T}_{\beta\text{-tubulin}}$) between the *Sph*I and *Hin*dIII sites of pGEM3Zf (Promega), producing pSK2778. The $\mathbf{P}_{EF1\alpha}$::$\mathbf{C}_{YC3.60}$::$\mathbf{T}_{\beta\text{-tubulin}}$ construct, released from pSK2778 by *Eco*RI and *Hin*dIII double digestion, was cloned between *Eco*RI and *Hin*dIII sites of binary vectors pBHt2 (Mullins et al., 2001) and pBGt (Kim et al., 2011), resulting in pBHt2-YC3.60 (SK2780) and pBGt-YC3.60 (SK2828), respectively.

To follow the localization of CaM, the enhanced green fluorescent protein (eGFP) gene was fused at the 3′-end of the CaM ORF using a slightly modified double-Joint PCR and split marker method (Fu et al., 2006; Yu et al., 2004). Two regions of the CaM gene, 1.3 kb fragment corresponding to the 0.3 kb 5′ flanking region and ORF and 1.2 kb fragment of the 3′ flanking region, were amplified by PCR using primer pairs CaM-5F/CaM-5Rand CaM-3F/CaM-3R, respectively. A 2.7 kb fragment carrying eGFP::HygR was amplified from pSK2978 using primers pLC24gfpF and pLC24gfpR. A mixture of three PCR products (1.3 kb:2.7 kb:1.2 kb = 1:3:1) was used as a template for second round PCR with 10 min annealing time. The resulting PCR product was split into two overlapping fragments via the third PCR using the following primer pairs: CaM-5N/Hyg-H2 and CaM-3N/Hyg-H3. These two fragments were used for fungal transformation.

2.3. Transformation of fungi and plants

The YC3.60 gene construct (Nagai et al., 2004), cloned under the *F. verticillioides* elongation factor-1α gene promoter, was introduced into *M. oryzae*, *F. oxysporum*, and *F. graminearum*. An *Agrobacterium tumefaciens*-mediated transformation (ATMT) protocol (Mullins et al., 2001) with EHA105 carrying pBHt2-YC3.60 was used to express YC3.60 in O-685 and 4360-17-1. To select transformants, minimal medium amended with hygromycin B (50 μg/ml for O-685 and 250 μg/ml for 4360-17-1) was used. Protoplasts of *F. graminearum* PH-1, prepared as previously described (Kim et al., 2011; Lee et al., 2002), were mixed with DNA of pBGt-YC3.60 for transformation, and resulting transformants were se-

lected using 100 μg/ml of geneticin screened for strong fluorescence. Bright fluorescent transformants were subsequently assayed for growth and spore production (Supplementary Fig. 1). Virulence tests of transformants used in this study were performed on the highly susceptible cultivar Eunpamil for *F. graminearum* (Son et al., 2011), *Arabidopsis thaliana* ecotype Cvi-0 for *F. oxysporum* (Kim et al., 2011) and Nipponbare for *M. oryzae* (Valent and Chumley, 1991) as described previously to assure that transformation had not affected these traits (Supplementary Fig. 2).

One transformant each from O-685 (named as FSK561), 4360-17-1 (named as MSK327), and PH-1 (name as FSK604) was used for imaging $[Ca^{2+}]_c$ dynamics. *F. graminearum* transformants expressing CaM fused with eGFP at the C-terminus were generated using a modified double-Joint PCR and split marker method. The YC3.60 construct under the control of the 35S promoter in pGreenII (Monshausen et al., 2008) was used to transform *Arabidopsis thaliana* ecotype Cvi-0, which is highly susceptible to *F. oxysporum* O-685 (Kim et al., 2011), via the use of a floral dip method (Clough and Bent, 1998). Transformants of *A. thaliana* were selected by germinating the sterilized seeds from treated Cvi-0 plants on 0.5 or 1× Murashige and Skoog mineral salts medium (Sigma, St. Louis, MO) with 0.8% Phytagel (Sigma) amended with 30 μg/ml hygromycinB, 1% (w/v) sucrose and vitamins. The plates were incubated at 21 °C under continuous light conditions. At seven days post-inoculation, seedlings of transformant were transferred into plastic pots filled with potting mix (Peters Redi-Earth; Grace/Sierra Co., Milpitas, CA) for seed production. Several independent lines of transformant were self-fertilized two more generations to obtain homozygous lines.

2.4. Time-lapse microscopic imaging of $[Ca^{2+}]_c$ changes

For imaging $[Ca^{2+}]_c$ during spore germination and early stages of hyphal growth (up to 2 days post inoculation), 100 μl of 5×10^5 ml^{-1} spores were inoculated on the middle of single-welled Lab-Tek II chambered coverglass system (Nalgene Nunc, Naperville, IL) coated with 300 μl of Cell-Tak buffer (10 μl of BD Biosciences Cell-Tak™, 285 μl of 0.1 M sodium bicarbonate, and 5 μl of 1 N NaOH) to immobilize fungal spores on the coverglass surface. For imaging during later stages of growth, 100 μl of 5×10^5 ml^{-1} conidia were inoculated on 2% or 4% potato dextrose agar (PDA; *M. oryzae*, *F. oxysporum* and *F. graminearum*) or Vogel's agar (for *F. oxysporum*) and grown at room temperature under continuous light. Square blocks of medium (1 cm × 1 cm), cut from leading edges of culture, were inverted onto a 20 μl drop of PDB in the single-welled Lab-Tek II coverglass chamber. To image changes of $[Ca^{2+}]_c$ in *M. oryzae* during spore germination and appressorium formation on cover glass, 100 μl of 2×10^5 ml^{-1} conidia of MSK327, resuspended in PDB amended with 2 μg/mL 1,16-hexadecanediol (from 0.5 mg/ml stock solution in 0.4% DMSO) to induce appressorium formation, was dropped in the single-welled Lab-Tek II coverglass chamber and imaged.

Seedlings of *A. thaliana* ecotype Cvi-0 were grown and inoculated with *F. oxysporum* O-685 expressing YC3.60 in single-welled Lab-Tek chambered coverglass system with 0.5× strength Arabidopsis Nutrient agar (0.7%) as previously described (Czymmek et al., 2007). Leaves of two-week old rice variety Nipponbare were surface inoculated with100 μl of 2×10^5 ml^{-1} conidia of MSK327 at 3 h post-inoculation, inoculated leaf sections were cut, placed on the Lab-Tek II coverglass chamber, and imaged to follow $[Ca^{2+}]_c$ changes as the fungus germinated, formed appresoria, and/or penetrated rice epidermal cells.

Time-lapse imaging was performed on a Zeiss LSM 5 DUO laser scanning confocal microscope with a 40× oil Plan-NeoFluor (1.3 numerical aperture) objective lens. Images were acquired using a 25 mW argon ion laser at a wavelength of 458 nm with the laser attenuated to prevent photobleaching. Images from three channels for YFP, CFP, and transmitted light plus an online ratio image of YFP/CFP with background subtraction were acquired. The pinholes for the YFP and CFP channels were set to a 1000 μm diameter and gain/offsets adjusted to yield a ratio near 1 in the cell cytoplasm. Images were acquired at 1.33–8.41 s intervals depending on frame-size. For ratiometric Ca^{2+} imaging only, 465–510 nm band pass and 530 nm long pass emission filters were used for CFP and YFP FRET signals, respectively. For dual label experiments with YC3.60 and the lipophilic membrane probe FM4-64FX (Invitrogen, Carlsbad, CA), 458 nm and 561 nm excitations were used with 465–510 nm band pass, 520–555 band pass and 630 long pass emission filters for CFP, YFP FRET and FM4-64FX, respectively. The following functions were performed by the LSM 510 AIM software (Rel. 4.2) for post-acquisition ratiometric processing: A 3 × 3 Gaussian lowpass filter was used to reduce noise after the simple ratio image was generated, a rainbow color look up table was applied and subsequent images were linearly rescaled via a ramp function for visualization of small ratio changes (Supplementary Fig. 14). Once appropriate imaging conditions were established *in vitro*, the same imaging conditions were utilized *in planta*. For long time-lapse (>1 h) imaging, we utilized the Multi-Time Macro to periodically autofocus the hypha of interest. Due to significant leaf topography, Ca^{2+} imaging of *M. oryzae in planta* typically required *z*-stacks taking a total of 30 s/stack and subsequent maximum intensity projections to document Ca^{2+} changes.

2.5. Treatment with Ca^{2+} channel blockers and ionophores

To image $[Ca^{2+}]_c$ changes in the growing hyphae after treatments with Ca^{2+} channel blockers and ionophore, spores were inoculated on 4% PDA or Vogel's agar in Ibidi μ-wells (2 × 9 μ-well, uncoated; Ibidi, Verona, WI). Each well was administered with 20 μL of Vogel's liquid medium including either 40 μM Br-A23187 Ca^{2+} ionophore plus 100 μM $CaCl_2$, or 100 μM of 2-APB (2-aminoethoxidiphenylborate; CalBioChem, La Jolla, CA), an inhibitor of IP_3-induced Ca^{2+} release.

2.6. Measurement of mean Ca^{2+} ratio intensity and data periodicity

For each image in a time-lapse experiment, the Ca^{2+} ratio mean intensity was measured using ImageJ (http://rsb.info.nih.gov/ij/). By manually entering a user-defined start and end frame into the macro the mean intensity for each channel in the defined moving region of interest (ROI) for every slice was calculated and the values were exported into ImageJ's results view window. The Image J tip Tracking Macro text is shown in Supplementary Fig. 13.

For time series analysis using autocorrelation and Fourier analysis in order to investigate the periodicity, if any, of fungal $[Ca^{2+}]_c$, we used SYSTAT (Versions 12 and 13). Autocorrelation tests were performed to determine if time-lapse data was random or self-correlated with a preferred periodicity. The degree of correlation for data value was measured by a correlation coefficient as follows:

$$\rho_k = \frac{\sum_{i=1}^{N-k}(X_i - \overline{X})(X_{i+k} - \overline{X})}{\sum_{i=1}^{N}(X_i - \overline{X})^2}$$

X_i is the ith data point. $\overline{X}$ is the mean of all N data points. X_{i+k} is $i + k$ the data point. k is called a lag which is the distance moved from original data point. As k increases from zero to N, the correlation coefficient shows a degree of correlation at each lag point k. In general, a high correlation coefficient implies that the data exhibited periodicity. In addition, data was also measured by Fourier analysis to determine if there was a preferred frequency in Ca^{2+} signatures. This was achieved by transforming the data into frequency (1/s).

3. Results

3.1. Location of the yellow Cameleon (YC) YC3.60 overlaps with calmodulin (CaM) and the Spitzenkörper

Cameleon had a cytoplasmic distribution and a single intensely labeled spot at the hyphal apex and was not sequestered into vacuoles, aggregates or other organelles (Fig. 1A–D). Staining of the endocytotic vesicle population associated with the Spitzenkörper, the organizing center for hyphal growth and morphogenesis (Steinberg, 2007), with the lipophilic membrane marker FM4-64X (Fig. 1B) revealed the bright spot of YC3.60 was located centrally within the vesicle cloud in a position consistent with the Spitzenkörper actin core (Fig. 1C). CaM fused to GFP (CaM-eGFP) also had a cytoplasmic distribution with noticeable tip-associated spot, similar to YC3.60 (Fig. 1E). Close inspection also showed elevated levels of CaM-eGFP just behind the hyhal apex and small foci in distil regions consistent with spindle pole body (SPB) localization (Fig. 1F). The SPB foci were observed in all non-apical cells as well as CaM-eGFP association with the septum and septal pore (Fig. 1G–I).

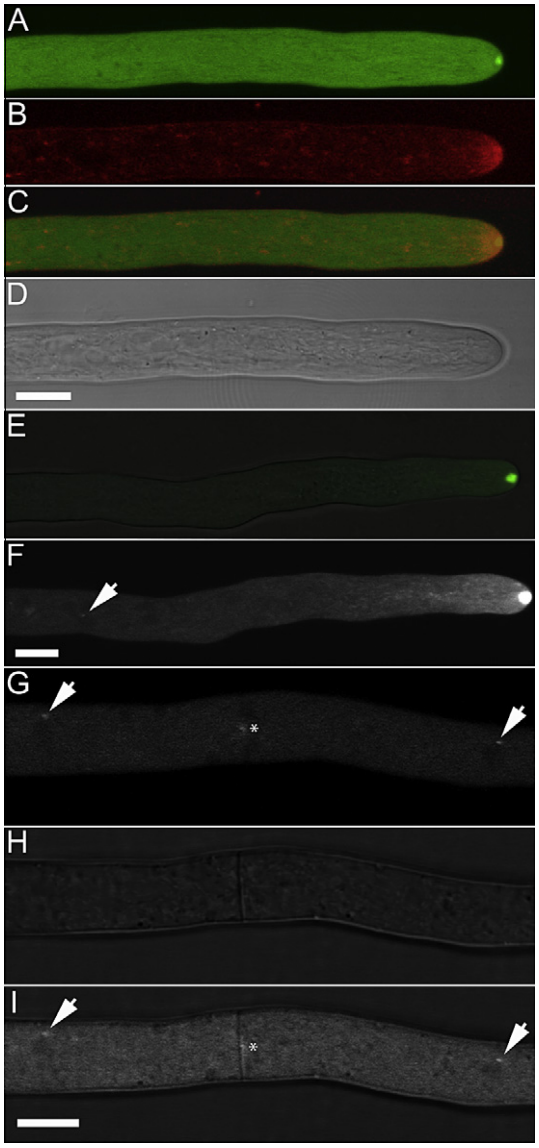

Fig. 1. Calmodulin and YC3.60 localization in *F. graminearum*. (A) YC3.60 showed uniform cytoplasmic distribution with a single bright spot located at hyphal tip apex. (B) FM4–64X labeling (red) of the same hypha revealed tip high accumulation of vesicles associated with the Spitzenkörper. (C) Overlay of (A) and (B) demonstrated that the YC3.60 spot appeared to localize at the Spitzenkörper core. (D) Differential interference contrast (DIC) image of hypha from (A–C). (E) Expression of CaM-EGFP showed a similar Spitzenkörper associated spot in this fluorescence/DIC overlay image. (F) Fluorescence only channel of (E) showed CaM-EGFP cytoplasmic distribution and distil spindle pole body associated foci (arrow). (G–I) Fluorescence, brightfield, and overlay images showed spindle pole body associated foci (arrowheads) and localization at the septum (asterisk). Scale bars = 5 μm. (For interpretation of the references to color in this figure legend, the reader is referred to the web version of this article.)

3.2. Ca^{2+} at the hyphal tip is pulsatile

To monitor the dynamics of intracellular free Ca^{2+} with minimal perturbation to the cells, we fine-tuned imaging conditions to optimize signal-to-noise without causing detectable photobleaching. After optimization, we could readily follow $[Ca^{2+}]_c$ dynamics in actively growing hyphae for 30 min to 1 h with an image acquired every few seconds (Figs. 2A, 3 and Supplementary Figs. 3A, 4, and 5). To determine the physical relationship of the Spitzenkörper to the tip high Ca^{2+} gradient observed, we utilized FM4-64X which clearly delineated the vesicular accumulation and small actin core devoid of vesicles (Compare Fig. 2A with 2B and Supplementary Fig. 3A with 3B). Although resolution of the ratiometric image was not sufficient to ascertain the precise boundary of the $[Ca^{2+}]_c$, gradient, high levels of $[Ca^{2+}]_c$ at the very apex correlated well with the Spitzenkörper (Fig. 2A and B, Supplementary Fig. 3A and B, and Supplementary movie 1). However, the $[Ca^{2+}]_c$ gradient clearly extended beyond the most dense vesicle accumulation at the hyphal tip. Time-lapse experiments revealed that the tip high $[Ca^{2+}]_c$ gradient was also pulsatile in nature (Fig. 3 and Supplementary movie 2, Supplementary Fig. 4 and Supplementary movie 3). Pulsatile $[Ca^{2+}]_c$ fluctuations within two actively growing hyphal tips of *F. oxysporum* (Fig. 3) also illustrated that the magnitude of $[Ca^{2+}]_c$ pulses varied significantly from cell-to-cell and within a single cell over a given period of time.

Utilizing a plugin created for Image J (Supplementary Fig. 13), we plotted ratiometric changes of $[Ca^{2+}]_c$ over time from a defined region of interest from the first 10 μm of the hyphal tip (Fig. 4). These plots over a 1000 s (16.67 min) period confirmed that the pulsatile nature of $[Ca^{2+}]_c$ at the hyphal tip was a general phenomenon in all three species but that their Ca^{2+} signatures were unique. For example, *F. graminearum*, the fastest growing (5.22 μm/min) had the most frequent and regular pulses, while *M. oryzae*, the slowest growing (3.05 μm/min) had the least regular pulses. Typically, the pulses in *M. oryzae* were of lower amplitude (ratio change 0.1–0.2) interspersed with occasional larger amplitude pulses. The growth rate of *F. oxysporum* was 3.66 μm/min with pulses being less frequent compared to *F. graminearum* and *M. oryzae*. Furthermore, the pulses were primarily restricted to the hyphal tip in all species, as measurements of distil regions (50–60 μm from the tip) of the same cell typically showed relatively static basal $[Ca^{2+}]_c$ levels (Supplementary Fig. 5).

In order to better understand the nature of tip-high $[Ca^{2+}]_c$ gradient and determine whether the maintenance of continuous gradient was a requirement for hyphal growth as suggested by earlier studies (Silverman-Gavrila and Lew, 2000, 2001, 2003), we imaged 10 different hyphae each of *F. oxysporum* and *M. oryzae* to find the location, extent and temporal nature of the gradient (Supplementary Fig. 6). For this analysis, we drew a line transecting the center of each hypha along the longitudinal axis and plotted the ratiometric change over distance (Supplementary Fig. 6A). The resulting line profiles from each hypha were averaged into a single profile. This $[Ca^{2+}]_c$ versus distance line profile was generated either when

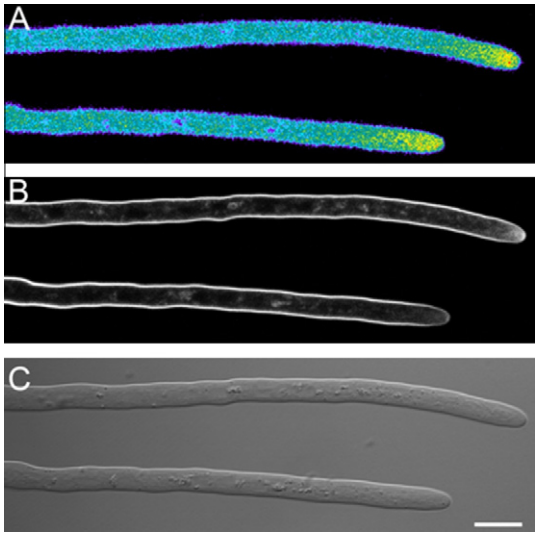

Fig. 2. Ratiometric imaging of subcellular Ca^{2+} in *F. oxysporum*. (A) YFP/CFP ratio showed intracellular Ca^{2+} was tip high at the apex of two adjacent hyphal tips. (B) FM4-64X labeling of vesicles at the Spitzenkörper showed overlap with tip high calcium in (A). (C) DIC image of (A) and (B). Scale bar = 10 μm.

hyphal tip $[Ca^{2+}]_c$ was at its maximum (Peak Profile) or when hyphal tip $[Ca^{2+}]_c$ was at its minimum (Valley Profile). The data showed that in both fungi, a rapid decrease in $[Ca^{2+}]_c$ concentration in the first 10 μm but the gradient often extended 20–30 μm from the tip when measured at the peak pulse (Supplementary Fig. 6B and C). However, a prominent gradient was not required to be maintained between pulses for growth to occur (Supplementary Fig. 6B and C).

3.3. Pulsatile Ca^{2+} signatures are age dependent

A comparison of germ tube tips at 6 h post-inoculation (hpi), young hyphae at 15 hpi and at 48 hpi demonstrated a lack of discernable repetitive pulsatile $[Ca^{2+}]_c$ at cell tips during the first two time points but were prominent at 48 hpi (Fig. 5). Sporadic large Ca^{2+} transients were observed in all ages. This data suggested that pulsatile $[Ca^{2+}]_c$ was age or developmentally dependent, which also was the case in *M. oryzae* (Fig. 8) and *F. oxysporum* (Fig. 6B and Supplementary movie 4). We sought to further characterize early stages of germ tube formation and development in *F. oxysporum* (Fig. 6A and B and Supplementary movie 4). One noticeable difference was basal levels of $[Ca^{2+}]_c$ in the spore was greater than young germ tube (compare inset Fig. 6 $T = 0.0$ h with $T = 3.71$ h and Fig. 6B). Furthermore, due to the small size of the germ tube, tip Ca^{2+} transients often propagated throughout the entire germ tube and into the spore at these early stages of development and frequently were elevated for longer periods (Fig. 6, $T = 3.72$–3.75 h). At later stages, presumably following septation, spores (Fig. 6, $T = 4.79$–4.8 h), and associated germ tubes exhibited independent Ca^{2+} transients that did not always propagate to adjacent cell compartments (Supplementary movie 4).

3.4. Periodicity in $[Ca^{2+}]_c$ pulses was observed in *F. graminearum* and *F. oxysporum*

We further examined the pulsatile nature of hyphal tip Ca^{2+} using time series statistical approaches (autocorrelation and Fourier analysis) to determine if there was any correlation or preferred frequency between pulses. First, we approximated the frequency of pulses in leading hyphae, by counting the number of peaks above background divided by total time. *F. graminearum* exhibited a

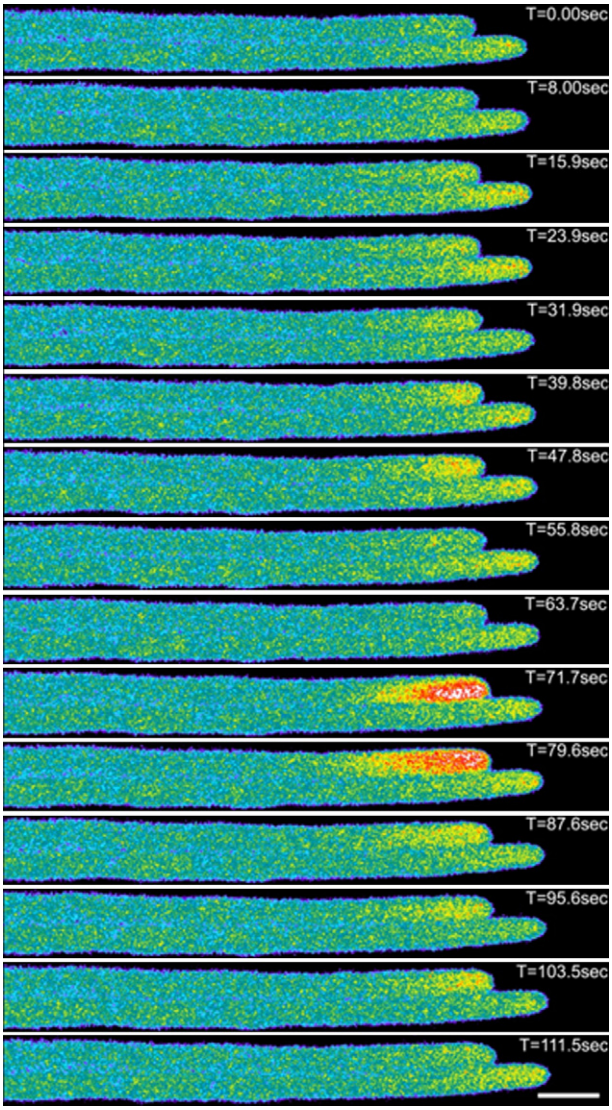

Fig. 3. Time-lapse ratiometric Ca^{2+} imaging of *F. oxysporum*. An approximately 2 min time-lapse image sequence of two adjacent hyphae which showed pulsatile cytoplasmic Ca^{2+} originating at hyphal tips with peak ratios at 47.8 s and 71.7 s for top hypha and 15.9 s, 47.8 s, 79.6 s, and 111.5 s for bottom hypha. Scale = 10 μm. See Supplementary movie 2.

$[Ca^{2+}]_c$ pulse on average every 14.6 s (range 8.1–18.8 s, total time analyzed = 6.05 h, 16 hyphae), *F. oxysporum* every 29.7 s (range 12.5–45.2 s, total time analyzed = 12.65 h, 19 hyphae) and *M. oryzae* every 22.4 s (range 12.4–30.0 s, total time analyzed = 5.15 h, 10 hyphae). Next we determined if the pulsatile Ca^{2+} was periodic using time-lapse autocorrelation analysis. For this, we acquired and analyzed time-lapse Ca^{2+} ratiometric data which exhibited both linear growth and level Ca^{2+} signatures (i.e., signature did not trend up/down/curve) for autocorrelation up to a lag of 50. *F. graminearum* frequently showed significant correlation of Ca^{2+} pulses as shown with this example with the first lag at 8 (14.2 s) and lag maxima at 8, 16, 28, 38, and 46 (Supplementary Fig. 7A). In *F. oxysporum,* although Ca^{2+} pulse correlation was documented with the first lag at 12 (31.8 s) and lag maxima at 12, 24, 36, and 48 (Supplementary Fig. 7B), this level of correlation was the exception when compared to the faster growing *F. graminearum*. In *M. oryzae* no significant peak correlation was ever observed (Supplementary Fig. 7C). While autocorrelation of Ca^{2+} pulses was observed with *F. graminearum* and *F. oxysporum*, Fourier analysis of

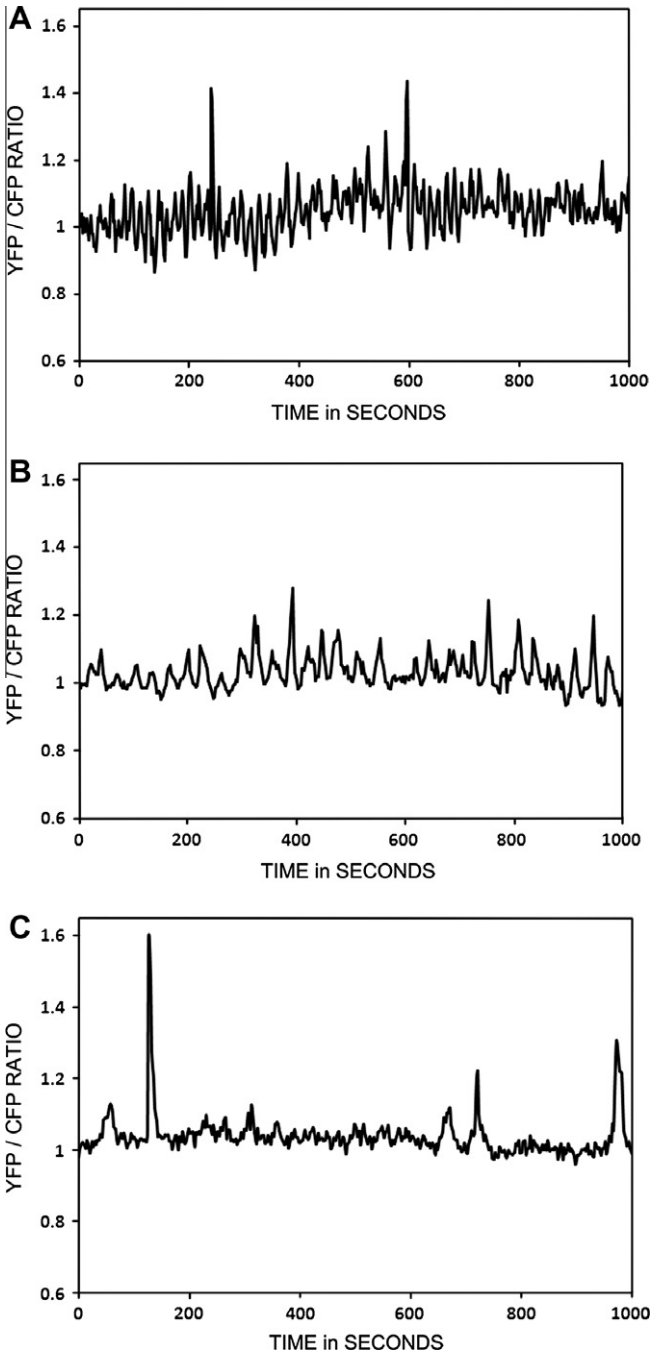

Fig. 4. Comparison of representative hyphal tip pulsatile Ca^{2+} signatures in *F. graminearum*, *F. oxysporum*, and *M. oryzae* over 1000 s period. (A) *F. graminearum* exhibited frequent low amplitude pulses with occasional high amplitude pulses. (B) *F. oxysporum* displayed less frequent and longer duration pulses compared to *F. graminearum*. (C) *M. oryzae* showed lower amplitude basal pulses compared to *Fusarium* spp. but interspersed with prominent large amplitude calcium transients. All starting time points were normalized to a ratio of 1.

time-lapse data never showed a dominant frequency for any of the three species tested.

3.5. Effects of 4-bromo-A23187 and 2-APB on Ca^{2+} Signatures

We determined the responsiveness of YC3.60 expressing fungal strains to pharmacological agents that are known to interfere with the Ca^{2+} signaling pathway in order to use them as a potential tool for analyzing the mechanism underpinning the generation of Ca^{2+} signatures. In *F. oxysporum*, we applied the Ca^{2+} ionophore 4-bromo-A23187 (40 μM) which enabled Ca^{2+} to cross the plasma membrane and resulted in a conspicuous alteration in the signature with a large amplitude-long duration Ca^{2+} influx, loss of pulsatile Ca^{2+} and concomitant cessation in growth (Supplementary Fig. 8A and Supplementary movie 5A). Interestingly, addition of 100 μM 2-APB, which is known to inhibit IP_3 (inositol 1,4,5-trisphosphate)-mediated Ca^{2+} release, resulted in multiple large amplitude transients and their subsequent decay, however hyphal growth continued unabated (Supplementary Fig. 8B and Supplementary movie 5B).

3.6. Ca^{2+} transients were observed during hyphal branching, septum formation, and cell–cell contact

Available data suggested the involvement of Ca^{2+} in controlling many cellular and developmental changes. For example, hyphal branching has been shown to be influenced by Ca^{2+} (Reissig and Kinney, 1983; Robson et al., 1991), and mutations in certain genes involved in Ca^{2+} signaling affected hyphal morphology (Brand et al., 2009; Chen et al., 2011; Nguyen et al., 2008). In *F. oxysporum*, branching is often associated with bifurcation of the tip (Fig. 7A). While low amplitude pulsation still occurred during the branching process, clear large amplitude transients were characteristic and surprisingly, occurred after short but prominent hyphal initials had already formed (Fig. 7A, T = 18.6 s and 24.8 s). Occasionally, tip branching would involve multiple large transients (Supplementary movie 6A). In *M. oryzae* hyphal branching typically occurred just behind newly formed septa (Fig. 7B and Supplementary movie 6B). In this case a very small extension was visible just behind the septum and shortly thereafter (Fig. 7B, T = 8.41 s) a prominent Ca^{2+} transient was observed on the distil side of the septum while a second smaller pulse was observed at T = 25.2 s. In both *F. oxysporum* and *M. oryzae*, these branching-related multiple transients were often characterized by far greater magnitude changes in the Ca^{2+} ratio and also propagated further back from branching region than steady state pulses observed at leading hyphal tips.

In both *F. oxysporum* and *M. oryzae*, a localized $[Ca^{2+}]_c$ transient was observed prior to the appearance of visible septum with variable time periods between the transient and septum appearance, ranging from 0.5 min to 5 min. At T = 0 s of a time series in *F. oxysporum* (Supplementary Fig. 9 and Supplementary movie 7), the transmitted light image showed no visible septum. At T = 10.63 s a single Ca^{2+} pulse approximately 100 μm away from the hyphal tip was observed, and within the next 40 s, a septum was visible. A similar pattern was also observed in *M. oryzae*.

Large amplitude Ca^{2+} transients were also affiliated with direct cell–cell contact (Supplementary Fig. 10). These transients typically had greater amplitude $[Ca^{2+}]_c$ changes than those at the tip (Supplementary Fig. 10A, T = 17.7 s and 44.2 s, Supplementary Fig. 10C, T = 6.19 s). The first example showed a hyphal tip coming into contact with a stationary distal hypha of *F. oxysporum* induced a large amplitude hyphal tip $[Ca^{2+}]_c$ transient at the tip followed by a responding transient in the adjacent hypha. In a second example, a large distil transient occurred in one of two adjacent hyphae growing parallel to each other without stimulating a response in the second hypha (Supplementary Fig. 10C and Supplementary movie 8).

3.7. Ca^{2+} signatures during appressorium formation in M. oryzae

Some plant fungal pathogens form a specialized infection structure prior to host invasion (Perfect and Green, 2001). *M. oryzae* produces one such structure called the appressorium to breach the host epidermal layer (Howard and Valent, 1996). Gene functional studies suggested the involvement of Ca^{2+} signaling in *M. oryzae*

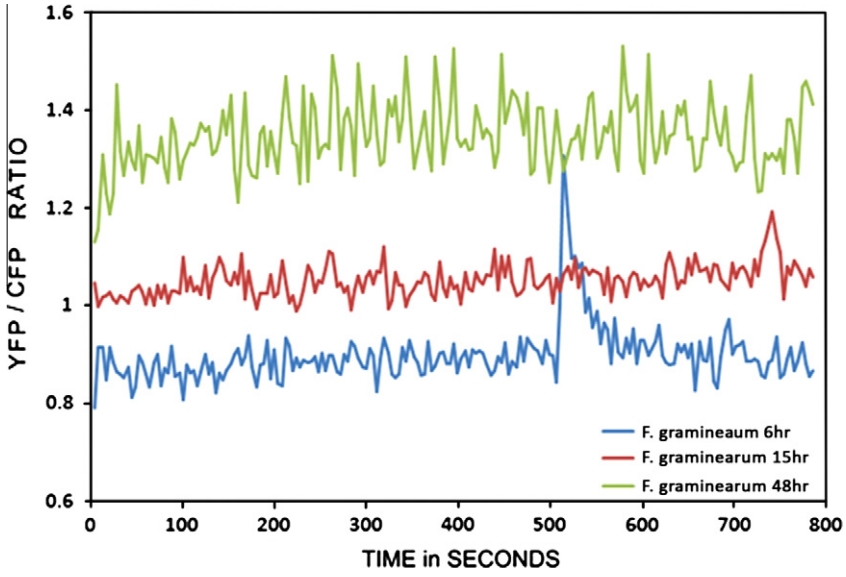

Fig. 5. Pulsatile Ca^{2+} signatures at the cell apex were age dependent. Germ tubes (blue) and young hyphae (red- less than 2 days old) of *F. graminearum* lacked discernable pulsatile $[Ca^{2+}]_c$ at cell tips as was typically observed in older rapidly growing hyphae (green). Although Ca^{2+} transients were observed in all ages, the more periodic larger amplitude pulsatile patterns were typically only observed in ~48 h post inoculation of spores onto media. (For interpretation of the references to color in this figure legend, the reader is referred to the web version of this article.)

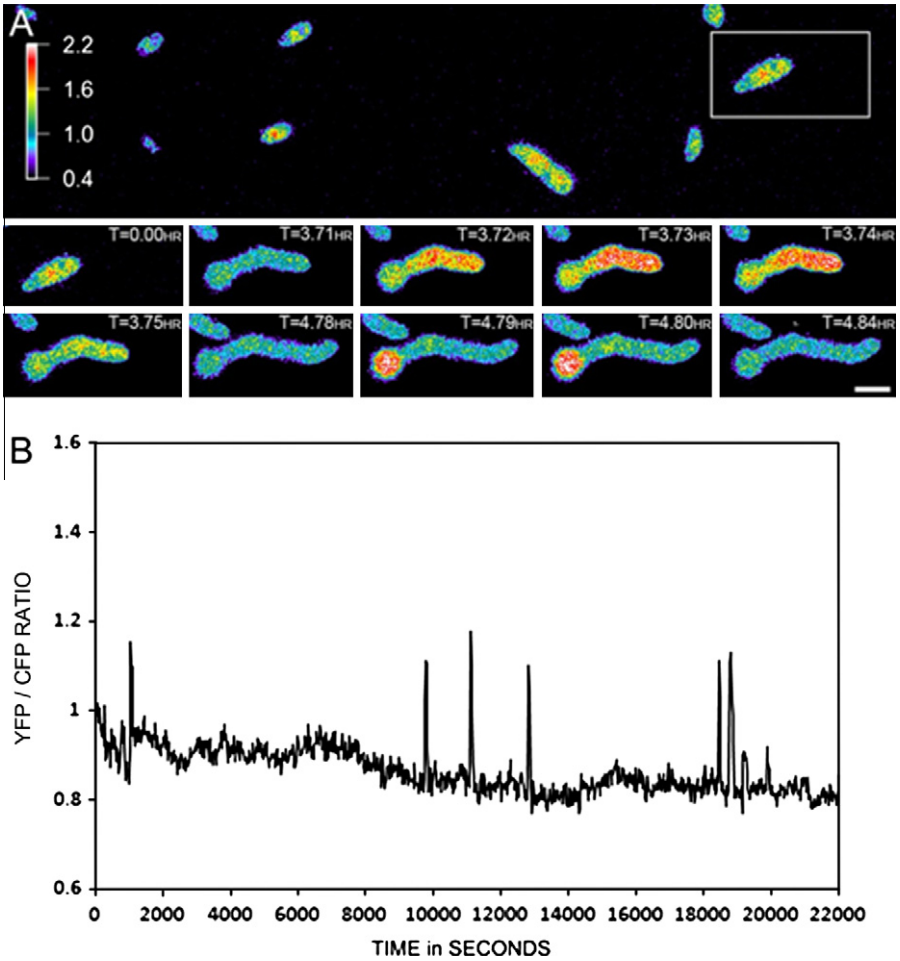

Fig. 6. Ca^{2+} signatures in *F. oxysporum* during spore germination and germ tube elongation. (A) Time-lapse analysis of calcium signatures in *F. oxysporum* during spore germination revealed occasional large amplitude transients but no discernable repetitive pulsatile pattern. Single germinating spore over 4.8 h period shows calcium transients extending through entire cell from $T = 3.73$ h to 3.75 h (Inset t-series). Also note calcium transients did not necessarily propagate to adjacent cell compartments ($T = 4.79$ h). Scale bar = 10 μm. (B) YFP/CFP ratio plot illustrated calcium signature pattern in (A) inset germ tube over entire 6.11 h. See Supplementary movie 4.

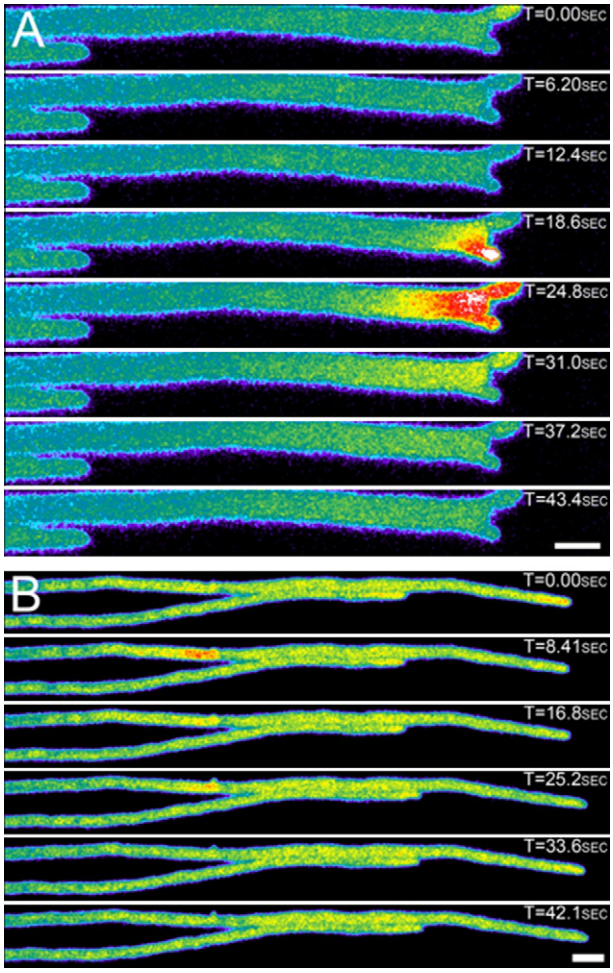

Fig. 7. Ca^{2+} transients correlated with hyphal branching in *F. oxysporum* and *M. oryzae*. (A) Time-lapse ratiometric calcium imaging of *F. oxysporum* during hyphal tip branching showed pulsatile Ca^{2+} with one to several large amplitude transients (T = 18.6 s and 24.8 s) following branch formation. (B) Multiple high amplitude calcium transients (T = 8.41 s and 25.2 s) also correlated to *M. oryzae* hyphal branch point immediately behind a previously formed septum. Scale bars = 10 μm. See Supplementary movies 6A and 6B.

appressorium formation (Choi et al., 2011; Nguyen et al., 2008). We imaged $[Ca^{2+}]_c$ changes during appressorial formation both *in vitro* and *in planta*. While pulsatile $[Ca^{2+}]_c$ was not observed in germ tubes in *M. oryzae* (Fig. 8 and Supplementary movie 9), as shown for *Fusarium* (Fig. 6), tip associated $[Ca^{2+}]_c$ transients affiliated with localized swelling as part of early appressorial formation were prominent (Fig. 8, T = 1.22 h and 1.28 h). Indeed, several large amplitude transients were documented through appressorial development over this 7.26 h sequence (Fig. 8 and Fig. 8 inset, T = 2.32 h, 2.91 h, and 3.25 h). Furthermore, basal levels of $[Ca^{2+}]_c$ within the appressorium were elevated (Fig. 8 inset yellow, T = 2.27 h, 2.38 h, 2.96 h, and 7.26 h), relative to the germ tube (Fig. 8 inset blue-green and Supplementary movie 9). Individual conidial cells also exhibited Ca^{2+} transients at various times during this sequence (Supplementary movie 9).

For *in planta* Ca^{2+} imaging of *M. oryzae*, the leaf topography presented special challenges. Namely, the lack of planarity required *z*-stacks and thus temporal information was reduced (Supplementary Fig. 11). Nevertheless, important insights were gained from these experiments with commonalities shared with the *in vitro* system including Ca^{2+} transients in appressoria (Supplementary Fig. 11 marked A, T = 0.0 h), conidia (Supplementary Fig. 11 marked C, T = 3.33 h) and germ tube tips (Supplementary Fig. 11, T = 3.75 h). It appeared however, that Ca^{2+} signatures *in planta* were more complex in conidia and especially germ tubes as they grew along the plant surface (Supplementary movie 10), likely due to much more heterogeneous chemical and physical environment on the rice leaf surface that the glass surface used for *in vitro* observation.

3.8. Ca^{2+} dynamics during *F. oxysporum*–*A. thaliana* interactions

Fusarium oxysporum is a root pathogen that colonizes the plant xylem, a water-conducting system, of its hosts, including *A. thaliana* (Czymmek et al., 2007; Kim et al., 2011). The resulting disruption of water and mineral transport causes the characteristic symptoms of wilting, vascular discoloration, and death of aerial tissues (Di Pietro et al., 2003). In the setup optimized to monitor time-lapse *in vivo* infection process without disrupting roots (Czymmek et al., 2007), we observed $[Ca^{2+}]_c$ pulses in a hypha of *F. oxysporum* contacting the root surface of *A. thaliana* ecotype Cvi-0 expressing YC3.60 (Supplementary Fig. 12). This ecotype is highly susceptible to *F. oxysporum* strain O-685 (Czymmek et al., 2007; Kim et al., 2011). In this case, within 35 s of contact with the epidermal root, a *F. oxysporum* hyphal tip exhibited a large pulse (Supplementary Fig. 12, T = 35.4 s) followed by a second smaller pulse (Supplementary Fig. 12, T = 88.5 s) and return to steady state (Supplementary movie 11). We were unable to detect any unusual large amplitude Ca^{2+} transients for 30 min prior to host-pathogen contact as the fungus approached. Furthermore, a concomitant $[Ca^{2+}]$ response was observed in *A. thaliana* cytoplasm (Supplementary Fig. 12. T = 35.4 s) and remained elevated for the duration of this sequence. We also determined that *F. oxysporum* hyphae exhibited tip high Ca^{2+} pulses within vascular tissues of *A. thaliana* as with *in vitro* experiments. Clear tip high pulsatile Ca^{2+} was observed (Fig. 9 and Supplementary movie 12). However, *in planta* pulses were far less regular and less well-defined than those observed during *in vitro* growth (compare Fig. 9 with Fig. 4B).

4. Discussion

4.1. Expression of YC3.60 provided novel insights into the nature of spatial and temporal dynamics of $[Ca^{2+}]_c$ in fungi

The Ca^{2+} signaling pathway has been shown to control spore production and germination (Choi et al., 2011; Shaw and Hoch, 2001), hyphal growth and differentiation (Brand et al., 2009; Chen et al., 2011), sexual development (Cavinder et al., 2011; Hallen et al., 2007), circadian rhythm (Yang et al., 2001), toxin biosynthesis (Chung, 2003), appressorium formation (Choi et al., 2011, 2009), and pathogenesis in both plants and animals (Bowman et al., 2009; Nguyen et al., 2008; Steinbach et al., 2006). Rapidly increasing fungal genome sequences have facilitated systematic identification of genes involved in Ca^{2+} signaling (Nguyen et al., 2008; Rispail et al., 2009; Zelter et al., 2004), and the functions of some of these genes have been characterized via targeted mutagenesis (Choi et al., 2011; Nguyen et al., 2008; Soriani et al., 2008). However, a major void in fungal Ca^{2+} signaling mechanisms exists, because visualization of $[Ca^{2+}]_c$ dynamics in fungal cells at the single cell level has been hampered by a number of significant technical challenges.

Fluorescent dyes such as Indo-1 and Fura-2 have been widely used for imaging intracellular Ca^{2+} in animals and plants due to the advantage of dual-wavelength for ratio imaging. However, their application in fungal cells has been very limited due to: (i) leakage of the loaded dye, (ii) rapid sequestration within non-targeted organelles, and (iii) poor intracellular loading because of rapid conversion to membrane-impermeable forms by cell wall esterases. Similar to aequorin, these dyes have been used mainly

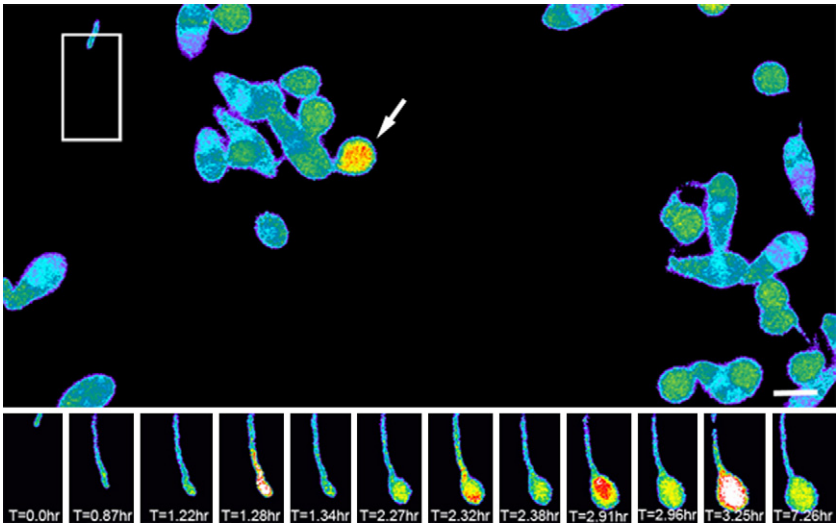

Fig. 8. Ca^{2+} transients in *M. oryzae* during appressorial development on an artificial surface. Ca^{2+} transients were observed in germ tubes, appressoria (arrow), and conidia on glass, although tip high gradients were only present during the occasional Ca^{2+} transients (inset $T = 1.28$ h). Time-lapse sequence of inset over 7.26 h illustrated large calcium transients at $T = 1.28$ h, $T = 2.32$ h, $T = 2.91$ h, and $T = 3.25$ h. Also note the elevated basal calcium levels (yellow) at $T = 2.27$ h, $T = 2.38$ h, $T = 2.96$ h, and $T = 7.26$ h compared to blue/green in germ tube at $T = 0.87$ h. Scale bar = 10 μm. See Supplementary movie 9. (For interpretation of the references to color in this figure legend, the reader is referred to the web version of this article.)

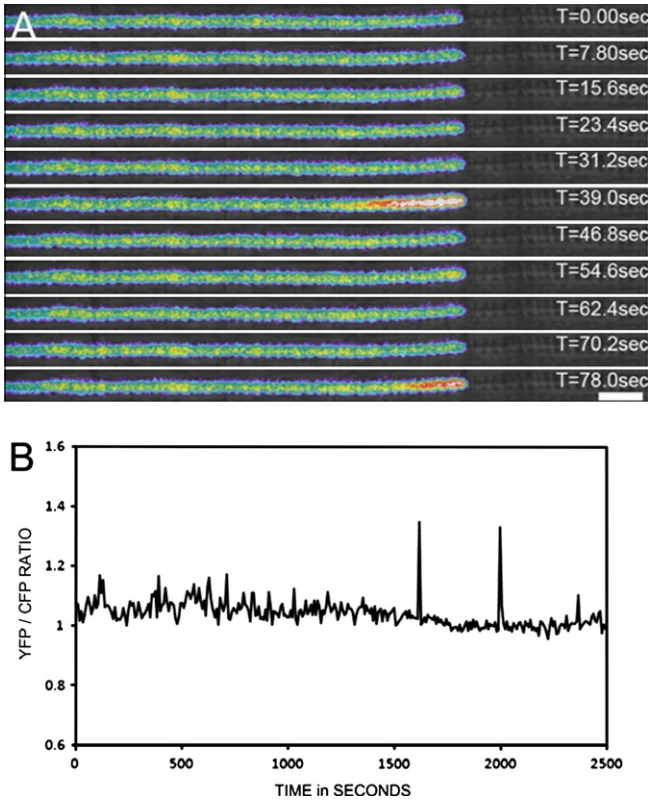

Fig. 9. Pulastile Ca^{2+} was observed *F. oxysporum* hyphae growing through the root xylem of *A. thaliana*. (A) Tip high pulsatile Ca^{2+} was observed as *F. oxysporum* hyphae grew within in *A. thaliana* root vascular tissue with peaks at $T = 15.6$ s, $T = 39.0$ s, $T = 54.6$ s, and $T = 78$ s. Scale bar = 10 μm. (B) Tracking and plotting the hyphal tip YFP/CFP calcium ratio from (A) dataset, showed pulsatile nature over a 2500 s time-lapse sequence. See Supplementary movie 12.

to monitor collective $[Ca^{2+}]_c$ changes in populations of fungal cells, and imaging of rapid Ca^{2+} dynamics in individual cells was not employed or practical. Because data from cell populations or tissues only show averaged patterns of Ca^{2+} change, alternative tools are needed to monitor rapid subcellular Ca^{2+} changes in individual cells and subcellular variation to understand how Ca^{2+} and signaling proteins change in response to specific stimuli.

Expression of YC3.60 permitted for the first time in fungi the ability to image and compare the rapidly changing spatial and temporal patterns of $[Ca^{2+}]_c$ both *in vitro* and *in planta* at the sub-cellular level. The cytoplasmic distribution pattern of YC3.60 overlapped with that of CaM with both proteins forming a single large apical spot within the vesicle cloud of the Spitzenkörper (Fig. 1), supporting that YC3.60 can serve to accurately reveal dynamic $[Ca^{2+}]_c$ changes to which CaM, components of the Spitzenkörper and other cellular machineries are exposed.

The spatial and temporal dynamics of $[Ca^{2+}]_c$ provided a number of novel findings for fungal Ca^{2+} signaling, one of which was the pulsatile nature of the tip-high $[Ca^{2+}]_c$ gradient in actively growing hyphae (Figs. 2–4 and Supplementary Figs. 3 and 4). It has been shown that polarized animal and plant cells, such as fibroblasts, neurons, root hairs and pollen tubes, also display a pulsatile pattern of $[Ca^{2+}]_c$ (Cardenas et al., 2008; Monshausen et al., 2008), but in fungi, our study is the first to demonstrate pulsatile tip high $[Ca^{2+}]_c$. The pulsatile $[Ca^{2+}]_c$ change conserved in these three kingdoms suggests that this process is a very ancient regulatory mechanism underpinning polarized cell growth. Loss of pulsatile signatures and cessation of growth in *F. oxysporum* (Supplementary Fig. 8A and Supplementary movie 5A) and similar changes of root hairs (Monshausen et al., 2008) after application of the Ca^{2+} ionophore Br-A23187 are consistent with this supposition.

Another notable finding was that the Ca^{2+} signatures in three species were consistently distinct (Fig. 4). *F. graminearum*, the fastest growing, exhibited the most regular pulses (peak approximately every 14.6 s) with occasional high amplitude pulses. In *F. oxysporum*, pulses were less frequent and less regular (peak approximately every 29.7 s) compared to *F. graminearum*. *M. oryzae*, the slowest growing, displayed lower amplitude and noisier pulses interspersed with occasional large pulses compared with the two *Fusarium* species. However, the pulsing frequency in *M. oryzae* was faster than that of *F. oxysporum* with a peak approximately every 22.4 s. Furthermore, in *F. graminearurm* and *F. oxysporum* these oscillations in some instances could be correlated (Supplementary Fig. 7A and B) and were thus not random, while

in *M. oryzae* temporal correlation of pulses was never observed. Whereas significant autocorrelation was common in *F. graminearum*, in *F. oxysporum* it was atypical. Autocorrelation analysis also revealed significant preferred peak lags that overall were consistent with manually derived average time between peaks (compare *F. graminearurm* 14.6 s vs autocorrelation 15.2 s; *F. oxysporum* 29.7 s vs autocorrelation 28.8 s). While this data demonstrated that under certain conditions, $[Ca^{2+}]_c$ peaks can be correlated, it must be noted that more often than not, the correlation was weak or in some cases non-existent, as with *M. oryzae*. This data serves to accentuate not only the species differences in $[Ca^{2+}]_c$ signatures, but also that hyphal tips are highly sensitive to local environmental cues.

The age-dependent nature of $[Ca^{2+}]_c$ signature at the cell apex (Figs. 5 and 6) also was a novel finding. Although Ca^{2+} transients were observed in all ages with YC3.60, the pulsatile patterns were typically only observed ~48 h post inoculation of spores onto media. Germ tubes and young hyphae lacked discernable $[Ca^{2+}]_c$ pulses at cell tips but exhibited occasional $[Ca^{2+}]_c$ transients (Figs. 5 and 6). Interestingly, in germinating spores of *F. oxysporum* and *M. oryzae*, we observed Ca^{2+} transients not only at the tip of germ tube but also inside the spore (Figs. 6 and 8, and Supplementary Fig. 11). One intriguing question is why the growth of mature hyphae is associated with pulsatile fluctuations of $[Ca^{2+}]_c$, while the growth of polarized germ tubes and young hyphae lacked this phenomenon. Does this suggest that tip growth requires different types of $[Ca^{2+}]_c$ signature and Ca^{2+} signaling machineries depending on age? Are Ca^{2+} channels and transporters and ion pumps differentially expressed during different stages of growth? Genes involved in Ca^{2+} influx and efflux have been identified in many fungi, including the species analyzed in our study (Rispail et al., 2009; Zelter et al., 2004), and analyzing their expression patterns in time and space should help answer these questions.

4.2. Fungal growth and the tip high Ca^{2+} gradient

A number of investigators (Jackson and Heath, 1993; Lew, 1999; Silverman-Gavrila and Lew, 2001, 2003) have analyzed hyphal growth of fungi or the water mold *Saprolegnia ferax* in light of hyphal Ca^{2+} using dual Ca^{2+} indicator dyes and suggested maintenance of a tip-high $[Ca^{2+}]_c$ gradient as a requirement for continued hyphal growth. In our analysis, although $[Ca^{2+}]_c$ pulses at the growing hyphal tip created such a gradient in all three species, the gradient was not required between pulses (Supplementary Fig. 3). In addition, polarized germinating conidia and many young hyphae (even with a Spitzenkörper as assessed by FM4-64X or YC3.60 spot at hyphal tip) never exhibited detectable repetitive pulsatile $[Ca^{2+}]_c$ and displayed only occasional tip high transients, leading to much longer intervals between $[Ca^{2+}]_c$ gradients similar to young pollen tubes which also appeared to lack pulsatile $[Ca^{2+}]_c$ (Feijó et al., 2001; Iwano et al., 2004; Messerli and Robinson, 1997). Taken together, these results suggest that the presence of a tip high $[Ca^{2+}]_c$ gradient does not require continuous maintenance for growth. It is not possible to ascertain whether imaging or dye loading conditions prevented this observation previously.

Considering our data demonstrated pulsatile behavior more consistently in older hyphae, an obvious question is what role pulsatile $[Ca^{2+}]_c$ plays in growth. The $[Ca^{2+}]_c$ gradient resulting from pulses extended up to 30 microns from the hyphal apex, but $[Ca^{2+}]_c$ concentrations decreased rapidly beyond the first 10 microns (Supplementary Figs. 5 and 6), and individual images in *N. crassa*, measured using Fluo-3 and Fura-Red micro-injection (Silverman-Gavrila and Lew, 2003), were comparable to what we observed. The overlap between $[Ca^{2+}]_c$ gradient and the Spitzenkörper is consistent with the prevailing model that change in $[Ca^{2+}]_c$ in response to external stimuli and tip expansion directs hyphal growth through interactions with various type of vesicles carrying building materials, the actin cytoskeleton and many other proteins (Jackson and Heath, 1993; Zelter et al., 2004). For example, Ca^{2+} ions have been known to regulate actin in a number of ways, binding directly to actin, changing the monomer synthesis or conformation and regulating the structure and the function of the actin network through a variety of actin-binding proteins (Adamikova et al., 2004; Holdaway-Clarke and Hepler, 2003). Therefore, hyphal tip Ca^{2+} signature likely plays an important role in regulating hyphal growth and morphogenesis through control of the apical actin network. Furthermore, our observation that germ tubes lacked detectable pulsatile $[Ca^{2+}]_c$ brings the intriguing possibility that the unique organization/structure/function of the germ tube plays (i.e., lack of Spitzenkörper) compared with the well-defined Spitzenkörper in faster growing older hyphae, plays a pivotal role in presence and/or activities of the $[Ca^{2+}]_c$ signaling protein machinery in these morphology distinct polarized cell tips. However, the lack of pulsatile signatures in many young hyphal tips with the apparent presence of a Spitzenkörper was a conundrum and it may suggest that key proteins and/or local environmental factors might be required for the calcium pulse to occur despite a conspicuous vesicle supply center. Exploring the subtle differences between younger and older hyphae in the context of calcium pulses or lack thereof, may not only help us elucidate their biological significance, but perhaps also deepen our understanding of Spitzenkörper organization.

Examination of data derived from plant pollen tube tip growth provides additional clues. The regular pulsatile fluctuation in growth rate of pollen tube tips has been noted (Cole and Fowler, 2006; Hepler et al., 2001; Holdaway-Clarke and Hepler, 2003). Furthermore, the oscillatory changes of Ca^{2+} and other ions in the cytoplasm were correlated with the pulsatile fluctuation in growth rate. Others also have shown the strong relationship between pulsatile $[Ca^{2+}]_c$ and pulsatile growth (Cardenas et al., 2008; Holdaway-Clarke and Hepler, 2003 #132; Monshausen et al., 2008). Thus, it is tempting to speculate that the reported pulsatile hyphal extension in filamentous fungi and water molds (López-Franco et al., 1994; Money, 2001, 2007) could be correlated with the $[Ca^{2+}]_c$ signatures we observed. However, the phenomenon of pulsed growth in fungi remains an area of debate since others (Sampson et al., 2003) observed no pulsatile growth of the hyphae of *N. crassa* and *S. ferax*, and modeling has suggested that helical growth could induce a measurement artifact based on the resolution limitations of optical microscopes (Jackson and Heath, 1993). Fortunately, ratiometric based pulsatile $[Ca^{2+}]_c$ measurements do not have the same measurement limitations as previous growth studies since they are based on intensity data at first 10 μm of tip. However, our available data was not sufficient to draw conclusions about this relationship, in part due to the same optical constraints reported previously for growth measurements and the very small increases in hyphal growth between $[Ca^{2+}]_c$ pulses. This is because the optical configuration needed to acquire sufficient fluorescent signals for ratiometric imaging, while maintaining cell viability without photobleaching over long time-lapse experiments, was not suitable for reliable growth measurements at the scale required. Likewise, measurements and correlation of pulsatile $[Ca^{2+}]_c$ with growth as done with pollen tubes (Ovečka et al., 2005; Parton et al., 2001) was not possible. Ultimately, due to their small size and relatively slow growth, accurately correlating growth rates with the rapid periodicity of $[Ca^{2+}]_c$ pulses in fungi will require an improvements in probes and/or instrumentation sensitivity.

In this study, we also tested suitability for pharmacological studies using the Ca^{2+} ionophore Br-A23187 and 2-APB to investigate the relationship between hyphal growth and $[Ca^{2+}]_c$ signature.

Br-A23187 induced a large amplitude and broad $[Ca^{2+}]_c$ transient with subsequent loss of pulsatile signatures and growth in *F. oxysporum* (Supplementary Fig. 8A). This response was consistent with other reports (Nelson et al., 2004; Robson et al., 1991). Use of 2-APB, which inhibits IP_3 receptors and activates TRP channels in a concentration dependent fashion (Bootman et al., 2002), induced high amplitude transients over a 2–3 min period (Supplementary Fig. 8B) and slowed but did not stop growth which illustrated the utility of subcellular temporal examination, as such transients would be averaged out in population analysis (Silverman-Gavrila and Lew, 2002).

4.3. Ca^{2+} transient is associated with key developmental and morphological events and cell–cell contact

The Ca^{2+} signatures associated with developmental and morphological events such as hyphal branching (Fig. 7), septation (Supplementary Fig. 9), and appressorium formation (Fig. 8 and Supplementary Fig. 11) were similar to those observed in tips of germinating spores and young hyphae; only sporadic large Ca^{2+} transients were observed. Transients associated with hyphal branching typically were far greater in magnitude and extended a longer distance compared with regular pulses observed at hyphal tips. Although the site and mode of hyphal branching was different between *F. oxysporum* (at the hyphal tip via bifurcation) and *M. oryzae* (behind newly formed septa), in both species these transients occurred after hyphal initials had formed (Fig. 7), suggesting the formation of hyphal initials triggered cellular changes leading to Ca^{2+} transients. Given that a new site of polarized growth is established in both branching and spore germination, similarity in $[Ca^{2+}]_c$ signature in both processes suggests the important role these transients play in establishing polarized tip growth.

In contrast to the order of $[Ca^{2+}]_c$ transient relative to the initiation of hyphal branching, an internally localized $[Ca^{2+}]_c$ transient was observed 0.5–5 minutes before the appearance of visible septum in both species (Supplementary Fig. 9), suggesting that the $[Ca^{2+}]_c$ transient may function to define the site of septum. However, considering that very early stages of cellular change during septum formation were not possible to detect under the imaging conditions used and that the interval between $[Ca^{2+}]_c$ transient and septum formation was very short (0.5 min) in some cases (e.g., Supplementary Fig. 9), it is possible that the $[Ca^{2+}]_c$ transient is a result rather than the cause of septum formation.

Cell–cell contact also caused a large amplitude $[Ca^{2+}]_c$ transient not only at the tip but also at distil regions (Supplementary Figs. 10A and 10C). We also demonstrated the occurrence of Ca^{2+} transients at both the host and fungal pathogen sides following a contact at the root surface (Supplementary Fig. 12). Early cell-signaling events play critical roles at both the pathogen and the host as the host attempts to ward off an invader while the pathogen maneuvers to exploit a nutrition source. Whether these contact-induced Ca^{2+} responses at both sides play roles in detecting and responding quickly remains to be investigated. Both types of physical contact led to similar patterns of Ca^{2+} response, suggesting the involvement of a mechano-sensing mechanism in both, but other possibilities (e.g., chemical induced response) cannot be ruled out.

4.4. Complex patterns of $[Ca^{2+}]_c$ change were observed during plant-fungus interactions

The appressorium of *M. oryzae* is essential for pathogenicity, because the high turgor pressure built in this dome-shaped structure drives penetration of the leaf surface (Howard and Valent, 1996). *In vitro*, as observed in germinating spores of *F. oxysporum* (Fig. 6), regularly pulsatile $[Ca^{2+}]_c$ was absent in germ tubes of *M. oryzae* (Fig. 8 and Supplementary movie 9). However, as the tip of germ tube swells, a differentiation process that proceeds appressorial formation, and forms an appressorium, multiple $[Ca^{2+}]_c$ transients were observed (Fig. 8). In addition, $[Ca^{2+}]_c$ transients were not limited to appressoria and the tip of germ tube but occurred in conidia too. However, for these transients we could not identify a particular or consistent sequence. On the leaf surface of rice, a complex pattern of $[Ca^{2+}]_c$ transients, with transients occurring in appressoria, conidia and germ tubes, was observed (Supplementary Fig. 11 and Supplementary movie 10). Consistent with the intimate association of $[Ca^{2+}]_c$ transients during appressorium formation in *M. oryze*, loss of function of many Ca^{2+} signaling genes affected appressorium formation and pathogenicity (Choi et al., 2009; Liu et al., 2009; Nguyen et al., 2008). Although clear tip high pulsatile $[Ca^{2+}]_c$ changes were observed in *F. oxysporum* hyphae growing within vascular tissues of *A. thaliana* (Fig. 9 and Supplementary movie 12), these pulses were far less regular and less well-defined than those observed during *in vitro* growth.

4.5. Fungi as models for the evolution of Ca^{2+} signaling and polarized growth

Even though the Ca^{2+} signaling pathway is well conserved, to execute idiosyncratic organism-specific cellular and developmental responses and to adapt to specific ecological niches, the Ca^{2+} signaling pathway likely has gone through evolutionary fine-tuning. The unique Ca^{2+} signatures in the three species support this hypothesis. With the means for imaging Ca^{2+} dynamics in individual cells, the genetic tractability of many fungi, and the availability of genome sequences from >100 species of fungi, we should be able to determine whether the evolutionary fine-tuning involves species-specific modification of the nature of $[Ca^{2+}]_c$ signatures, acquisition and/or loss of specific genes, changes in the expression, cellular location, and/or interactions of signaling components, or various combinations of these changes. Components of the fungal Ca^{2+} signaling pathway gleaned from genome sequences of selected species also revealed many features distinct from those in animals and plants (Rispail et al., 2009; Zelter et al., 2004). These results suggest that comparing the Ca^{2+} signaling mechanism in fungi with those in animals and plants will likely provide new insights into how this ancient cellular language has been modified in different kingdoms. Furthermore, filamentous fungi potentially serve as an excellent model for polarized growth and the role Ca^{2+} plays in this process. Polarized cellular growth is ubiquitous among all eukaryotes. While in plants and animals, polarized growth typifies only a few cell types (e.g., pollen tubes and root hairs in plants, neurons in animals), it predominates in fungi in the form of growing tips of spores and mycelium.

Acknowledgments

This work was supported by grants from the United States Department of Agriculture-NRI (2002-02367) and the National Science Foundation (MCB-1051667). We would like to thank Dr. Yin-Won Lee and Hokyoung Son at Seoul National University for conducting infection assays with *F. graminearum* PH-1 and one of its transformants expressing YC3.60. We would especially like to thank Dr. Richard J. Howard from The DuPont Company for many helpful discussions and suggestions for the manuscript.

Appendix A. Supplementary material

Supplementary data associated with this article can be found, in the online version, at http://dx.doi.org/10.1016/j.fgb.2012.05.011.

References

Adamikova, L., Straube, A., Schulz, I., Steinberg, G., 2004. Calcium signaling is involved in dynein-dependent microtubule organization. Molecular Biology of the Cell 15, 1969–1980.

Allen, G.J., Kwak, J.M., Chu, S.P., Llopis, J., Tsien, R.Y., Harper, J.F., Schroeder, J.I., 1999. Cameleon calcium indicator reports cytoplasmic calcium dynamics in *Arabidopsis* guard cells. Plant Journal 19, 735–747.

Bootman, M.D., Collins, T.J., Mackenzie, L., Roderick, H.L., Berridge, M.J., Peppiatt, C.M., 2002. 2-Aminoethoxydiphenyl borate (2-APB) is a reliable blocker of store-operated Ca^{2+} entry but an inconsistent inhibitor of InsP3-induced Ca^{2+} release. FASEB J. 16, 1145–1150.

Borst, J.W., Laptenok, S.P., Westphal, A.H., Kühnemuth, R., Hornen, H., Visser, N.V., Kalinin, S., Aker, J., van Hoek, A., Seidel, C.A.M., Visser, A.J.W.G., 2008. Structural changes of yellow cameleon domains observed by quantitative FRET analysis and polarized fluorescence correlation spectroscopy. Biophysical. J. 95, 5399–5411.

Bowden, R.L., Leslie, J.F., 1999. Sexual recombination in *Gibberella zeae*. Phytopathology 89, 182–188.

Bowman, B.J., Draskovic, M., Freitag, M., Bowman, E.J., 2009. Structure and distribution of organelles and cellular location of calcium transporters in *Neurospora crassa*. Eukaryotic Cell 8, 1845–1855.

Brand, A., Lee, K., Veses, V., Gow, N.A.R., 2009. Calcium homeostasis is required for contact-dependent helical and sinusoidal tip growth in *Candida albicans* hyphae. Molecular Microbiology 71, 1155–1164.

Cardenas, L., Lovy-Wheeler, A., Kunkel, J.G., Hepler, P.K., 2008. Pollen tube growth oscillations and intracellular calcium levels are reversibly modulated by actin polymerization. Plant Physiology 146, 1611–1621.

Cavinder, B., Hamam, A., Lew, R.R., Trail, F., 2011. *Mid1*, a mechanosensitive calcium ion channel, affects growth, development, and ascospore discharge in the filamentous fungus *Gibberella zeae*. Eukaryotic Cell 10, 832–841.

Chen, Y.-L., Brand, A., Morrison, E.L., Silao, F.G.S., Bigol, U.G., Malbas Jr., F.F., Nett, J.E., Andes, D.R., Solis, N.V., Filler, S.G., Averette, A., Heitman, J., 2011. Calcineurin controls drug tolerance, hyphal growth, and virulence in *Candida dubliniensis*. Eukaryotic Cell 10, 803–819.

Choi, J., Kim, Y., Kim, S., Park, J., Lee, Y.-H., 2009. *MoCRZ1*, a gene encoding a calcineurin-responsive transcription factor, regulates fungal growth and pathogenicity of *Magnaporthe oryzae*. Fungal Genetics and Biology 46, 243–254.

Choi, J., Kim, K.S., Rho, H.-S., Lee, Y.-H., 2011. Differential roles of the phospholipase C genes in fungal development and pathogenicity of *Magnaporthe oryzae*. Fungal Genetics and Biology 48, 445–455.

Chung, K.R., 2003. Involvement of calcium/calmodulin signaling in cercosporin toxin biosynthesis by *Cercosporanicotianae*. Applied and Environment Microbiology 69, 1187.

Clapham, D.E., 2007. Calcium signaling. Cell 131, 1047–1058.

Clough, S.J., Bent, A.F., 1998. Floral dip: a simplified method for Agrobacterium-mediated transformation of *Arabidopsis thaliana*. Plant Journal 16, 735–743.

Cole, R.A., Fowler, J.E., 2006. Polarized growth: maintaining focus on the tip. Current Opinion in Plant Biology 9, 579–588.

Coleman, J.J., Rounsley, S.D., Rodriguez-Carres, M., Kuo, A., Wasmann, C.C., Grimwood, J., Schmutz, J., Taga, M., White, G.J., Zhou, S., Schwartz, D.C., Freitag, M., Ma, L.-j., Danchin, E.G.J., Henrissat, B., Coutinho, P.M., Nelson, D.R., Straney, D., Napoli, C.A., Barker, B.M., Gribskov, M., Rep, M., Kroken, S., Molnar, I., Rensing, C., Kennell, J.C., Zamora, J., Farman, M.L., Selker, E.U., Salamov, A., Shapiro, H., Pangilinan, J., Lindquist, E., Lamers, C., Grigoriev, I.V., Geiser, D.M., Covert, S.F., Temporini, E., VanEtten, H.D., 2009. The Genome of *Nectria haematococca*: contribution of supernumerary chromosomes to gene expansion. PLoS Genetics 5.

Correll, J., Klittich, C.J.R., Leslie, J.F., 1987. Nitrate non-utilizing mutants of *Fusarium oxysporum* and their use in vegetative compatibility tests. Phytopathology 77, 1640–1646.

Cuomo, C.A., Guldener, U., Xu, J.-R., Trail, F., Turgeon, B.G., Di Pietro, A., Walton, J.D., Ma, L.-J., Baker, S.E., Rep, M., Adam, G., Antoniw, J., Baldwin, T., Calvo, S., Chang, Y.-L., DeCaprio, D., Gale, L.R., Gnerre, S., Goswami, R.S., Hammond-Kosack, K., Harris, L.J., Hilburn, K., Kennell, J.C., Kroken, S., Magnuson, J.K., Mannhaupt, G., Mauceli, E., Mewes, H.-W., Mitterbauer, R., Muehlbauer, G., Munsterkotter, M., Nelson, D., O'Donnell, K., Ouellet, T., Qi, W., Quesneville, H., Roncero, M.I.G., Seong, K.-Y., Tetko, I.V., Urban, M., Waalwijk, C., Ward, T.J., Yao, J., Birren, B.W., Kistler, H.C., 2007. The *Fusarium graminearum* genome reveals a link between localized polymorphism and pathogen specialization. Science 317, 1400–1402.

Czymmek, K.J., Fogg, M., Powell, D.H., Sweigard, J., Park, S.-Y., Kang, S., 2007. In vivo time-lapse documentation using confocal and multi-photon microscopy reveals the mechanisms of invasion into the *Arabidopsis* root vascular system by *Fusarium oxysporum*. Fungal Genetics and Biology 44, 1011–1023.

Dean, R.A., Talbot, N.J., Ebbole, D.J., Farman, M.L., Mitchell, T.K., Orbach, M.J., Thon, M., Kulkarni, R., Xu, J.-R., Pan, H., Read, N.D., Lee, Y.-H., Carbone, I., Brown, D., Oh, Y.Y., Donofrio, N., Jeong, J.S., Soanes, D.M., Djonovic, S., Kolomiets, E., Rehmeyer, C., Li, W., Harding, M., Kim, S., Lebrun, M.-H., Bohnert, H., Coughlan, S., Butler, J., Calvo, S., Ma, L.-J., Nicol, R., Purcell, S., Nusbaum, C., Galagan, J.E., Birren, B.W., 2005. The genome sequence of the rice blast fungus *Magnaporthe grisea*. Nature 434, 980–986.

Demaurex, N., 2005. Calcium measurements in organelles with Ca^{2+}-sensitive fluorescent proteins. Cell Calcium 38, 213–222.

Desjardins, A.E. (Ed.), 2006. *Fusarium* Mycotoxins, Chemistry, Genetics, and Biology. American Phytopathological Society Press, St. Paul, MN.

Di Pietro, A., Madrid, M.P., Caracuel, Z., Delgado-Jarana, J., Roncero, M.I.G., 2003. *Fusarium oxysporum*: exploring the molecular arsenal of a vascular wilt fungus. Molecular Plant Pathology 4, 315–325.

Diegelmann, S., Fiala, A., Leibold, C., Spall, T., Buchner, E., 2002. Transgenic flies expressing the fluorescence calcium sensor Cameleon 2.1 under UAS control. Genesis 34, 95–98.

Dodd, A.N., Kudla, J., Sanders, D., 2010. The language of calcium signaling. Annual Review of Plant Biology 61, 593–620.

Feijó, J.A., Sainhas, J., Holdaway-Clarke, T., Cordeiro, M.S., Kunkel, J.G., Hepler, P.K., 2001. Cellular oscillations and the regulation of growth: the pollen tube paradigm. BioEssays 23, 86–94.

Fu, J., Hettler, E., Wickes, B.L., 2006. Split marker transformation increases homologous integration frequency in *Cryptococcus neoformans*. Fungal Genetics and Biology 43, 200–212.

Hallen, H.E., Huebner, M., Shiu, S.-H., Güldener, U., Trail, F., 2007. Gene expression shifts during perithecium development in *Gibberella zeae* (anamorph *Fusarium graminearum*), with particular emphasis on ion transport proteins. Fungal Genetics and Biology 44, 1146–1156.

Hasan, M.T., Friedrich, R.W., Euler, T., Larkum, M.E., Giese, G.N., Both, M., Duebel, J., Waters, J., Bujard, H., Griesbeck, O., Tsien, R.Y., Nagai, T., Miyawaki, A., Denk, W., 2004. Functional fluorescent Ca^{2+} indicator proteins in transgenic mice under *TET* control. PLoS Biol. 2, e163.

Heim, N., Griesbeck, O., 2004. Genetically encoded indicators of cellular calcium dynamics based on troponin C and green fluorescent protein. Journal of Biological Chemistry 279, 14280–14286.

Hepler, P.K., Vidali, L., Cheung, A.Y., 2001. Polarized cell growth in higher plants. Annual Review of Cell and Developmental Biology 17, 159–187.

Higashijima, S., Masino, M.A., Mandel, G., Fetcho, J.R., 2003. Imaging neuronal activity during zebrafish behavior with a genetically encoded calcium indicator. Journal of Neurophysiology 90, 3986–3997.

Holdaway-Clarke, T.L., Hepler, P.K., 2003. *Tansley review* Control of pollen tube growth: role of ion gradients and fluxes. New Phytologist 159, 539–563.

Horikawa, K., Yamada, Y., Matsuda, T., Kobayashi, K., Hashimoto, M., Matsu-ura, T., Miyawaki, A., Michikawa, T., Mikoshiba, K., Nagai, T., 2010. Spontaneous network activity visualized by ultrasensitive Ca^{2+} indicators, yellow Cameleon-Nano. Nature Methods 7, 729–732.

Howard, R.J., Valent, B., 1996. Breaking and entering: host penetration by the fungal rice blast pathogen *Magnaporthe grisea*. Annual Review of Microbiology 50, 491–512.

Iwano, M., Shiba, H., Miwa, T., Che, F.-S., Takayama, S., Nagai, T., Miyawaki, A., Isogai, A., 2004. Ca^{2+} dynamics in a pollen grain and papilla cell during pollination of *Arabidopsis*. Plant Physiology 136, 3562–3571.

Jackson, S.L., Heath, I.B., 1993. Roles of calcium ions in hyphal tip growth. Microbiology and Molecular Biology Reviews 57, 367–382.

Kim, H.-S., Park, S.-Y., Lee, S., Adams, E.L., Czymmek, K., Kang, S., 2011. Loss of cAMP-dependent protein kinase A affects multiple traits important for root pathogenesis by *Fusarium oxysporum*. Molecular Plant–Microbe Interactions 24, 719–732.

Knight, M.R., Campbell, A.K., Smith, S.M., Trewavas, A.J., 1991a. Recombinant aequorin as a probe for cytosolic free Ca^{2+} in *Escherichia coli*. FEBS Letters 282, 405–408.

Knight, M.R., Campbell, A.K., Smith, S.M., Trewavas, A.J., 1991b. Transgenic plant aequorin reports the effects of touch and cold-shock and elicitors on cytoplasmic calcium. Nature 352, 524–526.

Kosuta, S., Hazledine, S., Sun, J., Miwa, H., Morris, R.J., Downie, J.A., Oldroyd, G.E.D., 2008. Differential and chaotic calcium signatures in the symbiosis signaling pathway of legumes. Proceedings of the National Academy of Sciences, USA 105, 9823–9828.

Lee, T., Han, Y.-K., Kim, K.-H., Yun, S.-H., Lee, Y.-W., 2002. *Tri13* and *Tri7* determine deoxynivalenol- and nivalenol-producing chemotypes of *Gibberella zeae*. Applied and Environmental Microbiology 68, 2148–2154.

Lew, R.R., 1999. Comparative analysis of Ca^{2+} an H^+ flux magnitude and location along growing hyphae of *Saprolegnia ferax* and *Neurospora crassa*. European Journal of Cell Biology 78, 892–902.

Liu, X.-H., Lu, J.-P., Dong, B., Gu, Y., Lin, F.-C., 2009. Disruption of *MoCMK1*, encoding a putative calcium/calmodulin-dependent kinase, in *Magnaporthe oryzae*. Microbiological Research 165, 402–410.

López-Franco, R., Bartnicki-Garcia, S., Bracker, C.E., 1994. Pulsed growth of fungal hyphal tips. Proceedings of the National Academy of Sciences, USA 91, 12228–12232.

Ma, L.-J., van der Does, H.C., Borkovich, K.A., Coleman, J.J., Daboussi, M.-J., Di Pietro, A., Dufresne, M., Freitag, M., Grabherr, M., Henrissat, B., Houterman, P.M., Kang, S., Shim, W.-B., Woloshuk, C., Xie, X., Xu, J.-R., Antoniw, J., Baker, S.E., Bluhm, B.H., Breakspear, A., Brown, D.W., Butchko, R.A.E., Chapman, S., Coulson, R., Coutinho, P.M., Danchin, E.G.J., Diener, A., Gale, L.R., Gardiner, D.M., Goff, S., Hammond-Kosack, K.E., Hilburn, K., Hua-Van, A., Jonkers, W., Kazan, K., Kodira, C.D., Koehrsen, M., Kumar, L., Lee, Y.-H., Li, L., Manners, J.M., Miranda-Saavedra, D., Mukherjee, M., Park, G., Park, J., Park, S.-Y., Proctor, R.H., Regev, A., Ruiz-Roldan, M.C., Sain, D., Sakthikumar, S., Sykes, S., Schwartz, D.C., Turgeon, B.G., Wapinski, I., Yoder, O., Young, S., Zeng, Q., Zhou, S., Galagan, J., Cuomo, C.A., Kistler, H.C., Rep, M., 2010. Comparative genomics reveals mobile pathogenicity chromosomes in *Fusarium*. Nature 464, 367–373.

Messerli, M.A., Robinson, K.R., 1997. Tip localized Ca^{2+} pulses are coincident with peak pulsatile growth rates in pollen tubes of *Lilium longiflorum*. Journal of Cell Science 110, 1269–1278.

Money, N.P., 2001. The pulse of the machine: reevaluating tip-growth methodology. New Phytologist 151, 553–555.
Money, N.P., 2007. Biomechanics of invasive hyphal growth. Biology of the Fungal Cell, 237–249.
Monshausen, G.B., Messerli, M.A., Gilroy, S., 2008. Imaging of the yellow Cameleon 3.6 indicator reveals that elevations in cytosolic Ca^{2+} follow oscillating increases in growth in root hairs of *Arabidopsis*. Plant Physiology 147, 1690–1698.
Mullins, E., Romaine, C., Chen, X., Geiser, D., Raina, R., Kang, S., 2001. *Agrobacterium tumefaciens*-mediated transformation of *Fusarium oxysporum*: an efficient tool for insertional mutagenesis and gene transfer. Phytopathology 91, 173–180.
Nagai, T., Sawano, A., Park, E.S., Miyawaki, A., 2001. Circularly permuted green fluorescent proteins engineered to sense Ca^{2+}. Proceedings of the National Academy of Sciences, USA 98, 3197–3202.
Nagai, T., Yamada, S., Tominaga, T., Ichikawa, M., Miyawaki, A., 2004. Expanded dynamic range of fluorescent indicators for Ca^{2+} by circularly permuted yellow fluorescent proteins. Proceedings of the National Academy of Sciences, USA 101, 10554–10559.
Nair, R., Raina, S., Keshavarz, T., Kerrigan, M.J.P., 2011. Application of fluorescent indicators to analyse intracellular calcium and morphology in filamentous fungi. Fungal Biology 115, 326–334.
Nakai, J., Ohkura, M., Imoto, K., 2001. A high signal-to-noise Ca^{2+} probe composed of a single green fluorescent protein. Nature Biotechnology 19, 137–141.
Nelson, G., Kozlova-Zwinderman, O., Collis, A.J., Knight, M.R., Fincham, J.R.S., Stanger, C.P., Renwick, A., Hessing, J.G.M., Punt, P.J., Van Den Hondel, C.A.M.J.J., Read, N.D., 2004. Calcium measurement in living filamentous fungi expressing codon-optimized aequorin. Molecular Microbiology 52, 1437–1450.
Nguyen, Q.B., Kadotani, N., Kasahara, S., Tosa, Y., Mayama, S., Nakayashiki, H., 2008. Systematic functional analysis of calcium-signaling proteins in the genome of the rice-blast fungus, *Magnaporthe oryzae*, using a high-throughput RNA-silencing system. Molecular Microbiology 68, 1348–1365.
Ovečka, M., Lang, I., Baluška, F., Ismail, A., Illeš, P., Lichtscheidl, I.K., 2005. Endocytosis and vesicle trafficking during tip growth of root hairs. Protoplasma 226, 39–54.
Palmer, A.E., Jin, C., Reed, J.C., Tsien, R.Y., 2004. Bcl-2-mediated alterations in endoplasmic reticulum Ca^{2+} analyzed with an improved genetically encoded fluorescent sensor. Proceedings of the National Academy of Sciences, USA 101, 17404–17409.
Parton, R.M., Fischer-Parton, S., Watahiki, M.K., Trewavas, A.J., 2001. Dynamics of the apical vesicle accumulation and the rate of growth are related in individual pollen tubes. Journal of Cell Science 114, 2685–2695.
Perfect, S.E., Green, J.R., 2001. Infection structures of biotrophic and hemibiotrophic fungal plant pathogens. Molecular Plant Pathology 2, 101–108.
Puhalla, J.E., 1985. Classification of strains of *Fusarium oxysporum* on the basis of vegetative compatibility. Canadian Journal of Botany 63, 179–183.
Read, N.D., Allan, W.T.G., Knight, M.R., Malho, R., Russell, A., 1992. Imaging and measurement of cytosolic free calcium in plant and fungal cells. Journal of Microscopy 166, 57–86.
Reissig, J.L., Kinney, S.G., 1983. Calcium as a branching signal in *Neurospora crassa*. Journal of Bacteriology 154, 1397–1402.
Rispail, N., Soanes, D.M., Ant, C., Czajkowski, R., Grünler, A., Huguet, R., Perez-Nadales, E., Poli, A., Sartorel, E., Valiante, V., Yang, M., Beffa, R., Brakhage, A.A., Gow, N.A.R., Kahmann, R., Lebrun, M.-H., Lenasi, H., Perez-Martin, J., Talbot, N.J., Wendland, J., Di Pietro, A., 2009. Comparative genomics of MAP kinase and calcium-calcineurin signaling components in plant and human pathogenic fungi. Fungal Genetics and Biology 46, 287–298.
Robson, G.D., Wiebe, M.G., Trinci, A.P.J., 1991. Involvement of Ca^{2+} in the regulation of hyphal extension and branching in *Fusarium graminearum* A 3/5. Experimental Mycology 15, 263–272.
Rogers, K.L., Picaud, S., Roncali, E., Boisgard, R., Colasante, C., Stinnakre, J., Tavitian, B., Brûlet, P., 2007. Non-invasive *in vivo* imaging of calcium signaling in mice. PLoS ONE 2, e974.
Sampson, K., Lew, R.R., Heath, I.B., 2003. Time series analysis demonstrates the absence of pulsatile hyphal growth. Microbiology 149, 3111–3119.
Shaw, B.D., Hoch, H.C., 2001. Ca^{2+} regulation of *Phyllosticta ampelicida* pycnidiospore germination and appressorium formation. Fungal Genetics and Biology 31, 43–53.
Silverman-Gavrila, L.B., Lew, R.R., 2000. Calcium and tip growth in *Neurospora crassa*. Protoplasma 213, 203–217.
Silverman-Gavrila, L.B., Lew, R.R., 2001. Regulation of the tip-high [Ca^{2+}] gradient in growing hyphae of the fungus *Neurospora crassa*. European Journal of Cell Biology 80, 379–390.
Silverman-Gavrila, L.B., Lew, R.R., 2002. An IP3-activated Ca^{2+} channel regulates fungal tip growth. Journal of Cell Science 115, 5013–5025.
Silverman-Gavrila, L.B., Lew, R.R., 2003. Calcium gradient dependence of *Neurospora crassa* hyphal growth. Microbiology 149, 2475–2485.
Son, H., Lee, J., Park, A.R., Lee, Y.-W., 2011. ATP citrate lyase is required for normal sexual and asexual development in *Gibberella zeae*. Fungal Genetics and Biology 48, 408–417.
Soriani, F.M., Malavazi, I., Da Silva Ferreira, M.E., Savoldi, M., Von Zeska Kress, M.R., De Souza Goldman, M.H., Loss, O., Bignell, E., Goldman, G.H., 2008. Functional characterization of the *Aspergillus fumigatus CRZ*1 homologue, *CrzA*. Molecular Microbiology 67, 1274–1291.
Souslova, E., Belousov, V., Lock, J., Stromblad, S., Kasparov, S., Bolshakov, A., Pinelis, V., Labas, Y., Lukyanov, S., Mayr, L., Chudakov, D., 2007. Single fluorescent protein-based Ca^{2+} sensors with increased dynamic range. BMC Biotechnology 7, 37.
Steinbach, W.J., Cramer Jr., R.A., Perfect, B.Z., Asfaw, Y.G., Sauer, T.C., Najvar, L.K., Kirkpatrick, W.R., Patterson, T.F., Benjamin Jr., D.K., Heitman, J., Perfect, J.R., 2006. Calcineurin controls growth, morphology, and pathogenicity in *Aspergillus fumigatus*. Eukaryotic Cell 5, 1091–1103.
Steinberg, G., 2007. Hyphal growth: a tale of motors, lipids, and the Spitzenkorper. Eukaryotic Cell 6, 351–360.
Sweigard, J.A., Carroll, A.M., Kang, S., Farrall, L., Chumley, F.G., Valent, B., 1995. Identification, cloning, characterization of *PWL2*, a gene for host-species specificity in the rice blast fungus. Plant Cell 7, 1221–1233.
Talbot, N., Foster, A., 2001. Genetics and genomics of the rice blast fungus *Magnaporthe grisea*: developing an experimental model for understanding fungal diseases of cereals. Advances in Botanical Research, 263–287.
Tallini, Y.N., Ohkura, M., Choi, B.-R., Ji, G., Imoto, K., Doran, R., Lee, J., Plan, P., Wilson, J., Xin, H.-B., Sanbe, A., Gulick, J., Mathai, J., Robbins, J., Salama, G., Nakai, J., Kotlikoff, M.I., 2006. Imaging cellular signals in the heart *in vivo*: cardiac expression of the high-signal Ca^{2+} indicator GCaMP2. Proceedings of the National Academy of Sciences, USA 103, 4753–4758.
Tian, L., Hires, S.A., Mao, T., Huber, D., Chiappe, M.E., Chalasani, S.H., Petreanu, L., Akerboom, J., McKinney, S.A., Schreiter, E.R., Bargmann, C.I., Jayaraman, V., Svoboda, K., Looger, L.L., 2009. Imaging neural activity in worms, flies and mice with improved GCaMP calcium indicators. Nature Methods 6, 875–881.
Truong, K., Sawano, A., Mizuno, H., Hama, H., Tong, K.I., Mal, T.K., Miyawaki, A., Ikura, M., 2001. FRET-based in vivo Ca^{2+} imaging by a new calmodulin-GFP fusion molecule. Nature Structural & Molecular Biology 8, 1069–1073.
Valent, B., Chumley, F.G., 1991. Molecular genetic analysis of the rice blast fungus, *Magnaporthe Grisea*. Annual Review of Phytopathology 29, 443–467.
Yang, Y., Cheng, P., Zhi, G., Liu, Y., 2001. Identification of a calcium/calmodulin-dependent protein kinase that phosphorylates the *Neurospora* circadian clock protein *FREQUENCY*. Journal of Biological Chemistry 276, 41064–41072.
Yu, J.-H., Hamari, Z., Han, K.-H., Seo, J.-A., Reyes-Domínguez, Y., Scazzocchio, C., 2004. Double-joint PCR: a PCR-based molecular tool for gene manipulations in filamentous fungi. Fungal Genetics and Biology 41, 973–981.
Zelter, A., Bencina, M., Bowman, B.J., Yarden, O., Read, N.D., 2004. A comparative genomic analysis of the calcium signaling machinery in *Neurospora crassa*, *Magnaporthe grisea*, and *Saccharomyces cerevisiae*. Fungal Genetics and Biology 41, 827–841.
Zhao, Y., Araki, S., Wu, J., Teramoto, T., Chang, Y.-F., Nakano, M., Abdelfattah, A.S., Fujiwara, M., Ishihara, T., Nagai, T., Campbell, R.E., 2011. An expanded palette of genetically encoded Ca^{2+} indicators. Science 333, 1888–1891.